COMPUTATIONAL STUDY OF HEAT TRANSFER ENHANCEMENT FOR A DIMPLED SURFACE IN A CHANNEL

by

ABHIJIT PARANJAPE

Presented to the Faculty of the Graduate School of

The University of Texas at Arlington in Partial Fulfillment

of the Requirements

for the Degree of

MASTER OF SCIENCE IN MECHANICAL ENGINEERING

THE UNIVERSITY OF TEXAS AT ARLINGTON

December 2012

Acknowledgements

I am extremely grateful to my advisor, Dr. Brian Dennis for providing valuable guidance and motivation for my thesis work. His knowledge helped me gain an insight not only in my research but in the field of CFD in general. I would also like to thank Dr. Kent Lawrence for sharing his valuable knowledge of meshing using ANSYS and taking time out to serve on my thesis committee. I am also thankful to Dr. Seiichi Nomura for serving on my committee and being an excellent graduate advisor.

I am heartily thankful to my CFD lab colleagues for their support and the knowledge that I have gained from the many discussions I had with them. I am also grateful to all my friends in UTA who have helped me immensely and made my time here an enjoyable one. I wish to thank the MAE administrative staff for their assistance during my time here.

Above all, I am indebted to my parents for providing me with words of encouragement, unconditional support and resources to pursue my graduate studies.

November 20, 2012

Abstract

COMPUTATIONAL STUDY OF HEAT TRANSFER ENHANCEMENT,

FOR A DIMPLED SURFACE IN A CHANNEL

Abhijit Paranjape, M.S.

The University of Texas at Arlington, 2012

Supervising Professor: Brian H. Dennis

Heat transfer augmentation techniques have gained great importance in different engineering applications to deal with thermal management issues. In this work, a numerical investigation was carried out to see the effects of spherical dimple arrays on heat transfer characteristics in a channel. These effects were observed for dimples on the bottom wall of the channel for laminar airflows. The effects of a 21×7 staggered array and a 19×4 inline array on the bottom wall were investigated using a 3D steady viscous computational fluid dynamics package with an unstructured grid. The heat transfer characteristics were studied as a function of the Reynolds number based on the hydraulic diameter of the channel. The channel height to dimple print diameter ratio was kept constant at H/D=1.0 while the dimple depth to dimple print diameter ratio was kept constant at δ/D=0.2. The heat transfer was quantified by computing the average heat transfer coefficient and Nusselt number. The pressure drop and flow characteristics were also calculated. The Nusselt number was compared with that of a smooth channel without dimples to assess the level of heat transfer enhancement provided by the dimples.

This investigation was carried out to observe if the use of dimples in a channel can enhance heat transfer characteristics without severe penalties associated with

pressure drops for laminar airflows. When compared with a smooth channel, the use of dimples enhanced heat transfer. It was also observed that the staggered array facilitates higher heat transfer augmentation when compared to the inline array.

Table of Contents

List of Illustrations

List of Tables

Chapter 1

Introduction

1.1 Background

Heat transfer enhancement techniques have gained increasing importance in different applications such as combustion chamber liners, internal cooling of turbine airfoils, heat exchangers and microelectronic cooling. Tremendous amount of research has been carried out in the recent past on thermal management issues. According to Mahureand et al [23] , heat transfer enhancement techniques can be broadly classified in to three main types viz., passive heat transfer enhancement techniques, active heat transfer enhancement techniques and compound techniques. The active method requires power from an external source for heat transfer enhancement. The use of magnetic fields, use of cams and plungers to induce pulsation are some of the many examples of active heat transfer enhancement techniques. The passive heat transfer enhancement methods consist of use of roughened or extended surfaces and many other geometric modifications to improve convective heat transfer enhancement. The compound method of heat transfer enhancement involves combined use of active as well as passive methods of heat transfer enhancements to achieve higher degree of heat transfer enhancement than with the use of any one method alone.

Passive techniques such as use of ribs, pin fins, vortex generators and dimples have been extensively studied to enhance heat transfer for different applications. Making the thermal boundary layer thinner or even breaking it can help in enhancing the convective heat transfer. This can be done by the introduction of disturbances in the flow by using the techniques mentioned above.

Dimples have been used on the golf ball for drag reduction [1]. These dimples on the golf balls help in transitioning the boundary layer upstream of the ball from laminar to

turbulent. This helps in giving a narrow separated flow region downstream of the ball and reduces form drag. The effect of using dimples on a golf ball compared to a smooth sphere is shown in Figure 1-1. [9]

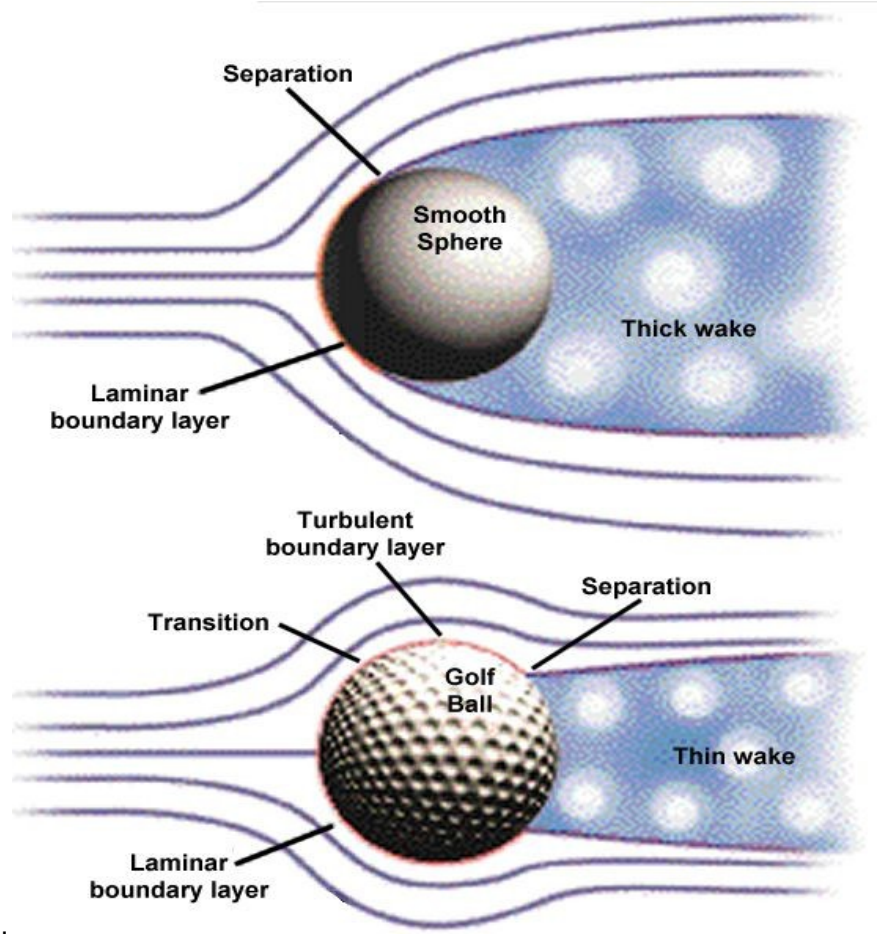

Figure 1-1 Comparison of flow over a smooth sphere and dimpled golf ball [9]

Recently, dimples have found their application in heat transfer augmentation techniques and not just for drag reduction. Heat transfer augmentation using techniques such as ribs, pin fins and vortex generators result in pressure drop penalties that severely affect the aerodynamic performance as these devices protrude in to the flow introducing

form drag. In comparison, the use of dimples has also shown to significantly improve heat transfer coefficient with lesser pressure drop penalties.

The key to enhancing convective heat transfer for any sort of heat sink is to draw cold fluid from outside the thermal boundary layer and get it into contact with the heated wall. According to Mahmood et al. [21], the use of dimples helps in heat transfer enhancement because it forms vortex structures and vortical fluid is shed from each individual dimple and it then advects downstream on the flat surface. Another reason for heat transfer augmentation in case of dimpled surface according to Mahmood et al. [21] is reattachment of the shear layer that forms on top of the dimple. The vortex like structures promote mixing of the cold fluid outside the thermal boundary layer into the hot fluid. The vortex structures over dimples as observed by Mahmood et al. [21] are shown in Figure 1-2

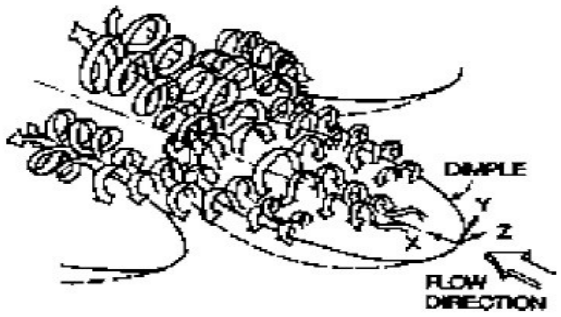

Figure 1-2 Vortex structures over dimples on a wall [21]

The increase in surface area due to the use of dimples is another important reason for heat transfer enhancement.

It is known from elementary aerodynamics that parasitic drag is the drag experienced by a body due to its motion in a fluid. The parasitic drag consists of form drag which is dependent on the form or shape of the body. Streamlined bodies will have

lesser form drag as compared to bodies with apparent higher cross sections. The parasitic drag also consists of skin friction drag and interference drag. Skin friction arises purely because of the friction prevalent between the surface of the body and moving fluid. Although no form drag is introduced due to the use of dimples, heat transfer enhancement is obtained at the cost of increase in skin friction drag. This is because of increase in the surface roughness. Hence, dimples are not primarily used for drag reduction in channels, but for the purpose of heat transfer augmentation. However, the total hydraulic losses in case of a dimpled surface are less than those in case of protruding devices like pin fins, ribs and vortex generators. Therefore, in applications like microelectronic cooling where space constraints are encountered, a smaller heat sink with dimples can be used to obtain the same level of heat transfer as a heat sink with smooth surface. The ease of manufacturing dimples on a surface compared to manufacturing other protruding devices is another reason why dimples are a more attractive proposition. In a heat sink, weight is another important consideration. The use of dimples should help in reducing the overall weight as material is scooped out for manufacturing of dimples. Thus, for heat sinks in microelectronic applications in specific, the objectives of space and weight reduction can be achieved more easily as compared to other methods. With the cost of the material as another parameter, optimization efforts can be undertaken for designing the heat sink. The analysis of a heat sink for microelectronic cooling and its redesign based on the observations by Silva et al [28] is good example of heat sink design for such applications considering all the important parameters.

In case of applications like internal cooling of turbine blades, the use of dimples alone may not suffice. According to Rao et al. [27], the use of dimples alone for heat sink in case of internal cooling of turbine blades in not sufficient to maintain the structural

integrity and stiffness of the cooling channel. However, according to Rao et al. [27], the use of a pin-fin array with dimples placed transversely between the pins in the array can help in achieving good thermal performance along with maintaining structural integrity and stiffness.

The next section deals with the literature review of the published literature from which the objective of this study will be defined.

1.2 Literature Review

Due to the increasing need to deal with thermal management issues, a lot of research effort has been dedicated to the use of dimples and other devices used for heat transfer enhancement in different engineering applications. Researchers have carried out experimental and numerical studies for the use of dimples. The use of dimples has attracted the attention of many researchers because of less hydraulic losses associated with their use. In the available literature, it can be seen that Reynolds number, channel height to dimple diameter ratio (H/D), dimple depth to dimple diameter ratio (δ/D), and dimple array geometry are the defining parameters in heat transfer enhancement effects. A typical arrangement of dimpled channel geometry as given by Doo et al [8] is shown in Figure 1-3

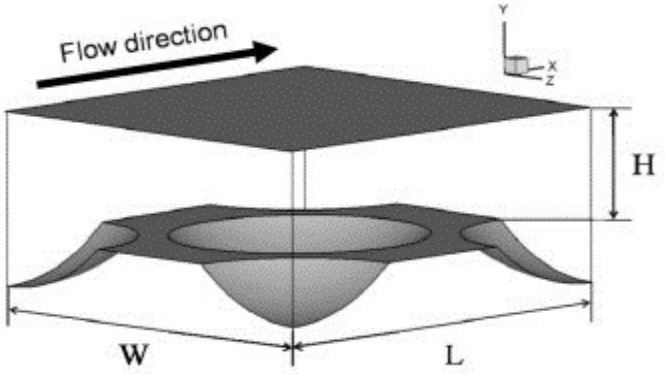

Figure 1-3 Typical arrangement of dimpled channel geometry [8]

Using these parameters, many investigations have been carried out for a rectangular channel with single or multiple dimpled walls.

Bearman and Harvey [4] carried out one of the earliest works on dimples by experimentally studying the effect of dimples on cylinders for drag reduction. These dimples on the cylinder reduce drag in the same way they do on the surface of a golf ball. Many earlier studies on dimples were carried out by Russian researchers. Afanasyev et al. [2] studied heat transfer and flow characteristics for flow over flat wall with regular arrays of spherical pits. Blen'kiy et al [20] studied effects of flows on a staggered array of dimples on the interior surfaces of cylinders .Gortyshov et al [34] studied effects of flows in narrow channel with the two opposite walls having spherical shaped dimples. High heat transfer augmentation rates as much as 1.5 times that of a smooth surface were reported in these studies.

In more recent studies, Chyu et al. [7] studied the effect of using hemispheric and tear drop shaped concavities in a channel to enhance heat transfer. The Reynolds number range studied was 10,000 to 50,000 at different H/D values of 0.5, 1.5, and 3. The heat transfer augmentations of 2.5 times that of a smooth channel were reported.

Moon et al. [24] carried out experiments to study the effect of channel height on heat transfer characteristics in a dimpled channel. The Reynolds number range studied was 12,000 to 60,000 and H/D values of 0.37, 0.74, 1.11, and 1.49 were studied. It was shown that the heat transfer enhancement did not change with respect to the channel height when it was greater than the dimple depth. Mahmood et al. [22] carried out experiments on a dimpled surface placed on the wall of a channel in the Reynolds number range from 600 to 11,000 and ratios of air inlet stagnation temperature to surface temperature ranging from 0.78 to 0.94. Four different H/D ratios of 0.20, 0.25, 0.50 and 1.0 were tested while the δ/D ratio was kept at 0.2. It was shown that the vortex pairs shed periodically increase in strength and local Nusselt number increases as the non-dimensional channel height decreases. Burgess et al. [6] experimentally observed the effect of dimple depth to dimple print diameter ratio for δ/D values of 0.1, 0.2 and 0.3 and showed that the local Nusselt number and vortex strength increases with increasing δ/D ratios. Ligrani et al. [18] studied the effect of dimples and protrusions on opposite walls. It was shown that protrusions enhance heat transfer because of the strong secondary vortex pairs from each dimple especially from the dimple rim and diagonal edges and which then advect over the flat surface downstream. Bunker et al. [5] studied the effects for turbulent flow in the Reynolds number range of 20,000 to 90,000 inside circular tube with an in-line array of dimples. Effects for different dimple array densities were also studied. For the case of array density greater than 0.5 and dimple depth to diameter ratio greater than 0.3, heat transfer enhancements two times that of a smooth circular tube were observed. The friction factor increase observed was 4 to 6 times greater than that observed for smooth tubes. Terekhov et al. [30] [31] studied the effect of changes in cavity depth or contour of dimple on changes in flow characteristics. Dimples with δ/D ratio of 0.13 were studied and velocity and pressure profiles were shown. The flow

visualizations using gas bubbles were also shown. Xiao et al [33] experimentally studied the effect of an array of dimples on locally and spatially averaged Nusselt number distributions and on friction factors in channels. The study was carried out for laminar flows with Reynolds number varying from 260 to 1030 while two different δ/D ratios of 0.1 and 0.3 were tested. The combined effects of dimples and protrusions on opposite walls were also studied. It was reported that the trends shown by Nusselt number ratios and friction factor ratios are opposite for the ones observed for turbulent flows. However for friction factors, similar trends as those observed for fully turbulent flows are seen as the H/D and δ/D ratios are increased. The presence of protrusions on the top wall was shown to give lower Nusselt number ratio enhancements when compared to smooth top walls. Turnow et al. [32] investigated vortex structures and heat transfer mechanism of turbulent flows over a staggered array of dimples using Large Eddy Simulations and Laser Doppler Velocimetry. It was found that the maximum thermo-hydraulic performance was obtained for δ/D ratio of 0.26 while the heat transfer rate was enhanced up to 201% compared to a smooth channel. Han [10] investigated dimples in turbine blade cooling. Dimples were found to be a suitable choice because pressure drop was the primary design criteria. Small et al [29] carried out experimental and numerical studies on heat sinks with dimpled surfaces. The analysis resulted in a heat sink with a staggered array of 9,8 and 9 rectangular fins with dimples being the most efficient.

Simulations for a channel with hemispherical cavities on walls were carried out by Lin et al.[19] Isaev et al. [11] [12] [13] [14] [15] [16] studied the effect of dimple depth to diameter ratio from 0.06 to 0.24. The momentum and energy equations were solved with the SIMPLEC finite difference method using multi-block grids. Detailed studies of flow structure inside and in the wake area of dimples were carried out for dimples with δ/D=0.22. The studies were primarily concentrated on heat transfer and flow structure.

Park et al. [25] simulated flow over deep dimples in a channel with δ/D ratio of 0.3. The commercial CFD package Fluent 6.0.12 was used for the solutions. The results showed good agreement with the experiments. Kim [17] carried out optimization of dimple profile for turbulent flow and found optimum values of dimple depth to diameter ratio as 0.24 and relative pitch as 0.81 to 1.21.

From the published literature, it can be seen that there is a lot of experimental and numerical data available on the use of dimpled surfaces. However, there is a scarcity of literature available for computational work in the laminar flow regime. There is a need to gain a better insight in to the nature of laminar flows over dimpled surfaces. An investigation to see the effects of different array geometries is also needed. This study is carried out to see whether dimples can enhance heat transfer and thermal performance for laminar airflows in a narrow channel for two different array geometries using Computational fluid dynamics.

1.3 Thesis Outline

The background and literature review of heat transfer enhancement especially using dimpled surfaces was presented. In Chapter 2, the methodology that was used in this study that is CFD or Computational Fluid Dynamics is discussed. Chapter 3 deals with the Computational setup and solution strategy for the study. Chapter 4 presents CFD results and discussion about the observations. Chapter 5 contains the summary and conclusion for this work. Chapter 6 lists recommendations for future work that could be conducted with this investigation.

Chapter 2

Computational Fluid Dynamics Methodology

2.1 Introduction

Computational Fluid Dynamics better known as CFD is the process of solving mathematical models of different phenomenon in nature by using numerical methods. CFD can be applied to solve different engineering problems in Mechanical engineering, Chemical engineering, Environmental engineering and Bioengineering among many other fields. CFD has evolved as a third approach to problem solving in addition to pure theory and pure experiment. Many problems for which closed form analytical solutions are not possible or problems for which setting up experiments is costly or impractical can be solved by using CFD.

For problems associated with Fluid Mechanics and Heat Transfer, CFD can be used to solve the Navier-Stokes equations which are a coupled set of partial differential equations for which no closed form analytical solution has been found till date. The solution of Navier-Stokes equations for different fluid and thermal systems depends on the numerical application of boundary conditions for that particular system.

With the advancement of computer resources and continuous research on development of efficient solution methods, many problems which were considered complex can be easily solved with the use of CFD. The solution of blunt body problem as given by Anderson [3] using CFD is a good example of how problems which were considered unsolvable are now easily solved. In spite of all these advantages of CFD, it should be remembered that CFD cannot replace pure theory and pure experiment and that it can be only used to validate analytical and experimental results. This is because of the fact that many problems cannot be realistically modeled using CFD even today and that realistic solutions can only be found by theory or experiment. It should also be

remembered that CFD can be computationally expensive for setting up many complex problems and selection of this method depends on the available computer resources.

The process of solving a problem using CFD consists of the following steps in general.

2.1.1 Problem definition and modeling of geometry

Identification and creation of geometry based on the boundary conditions and operating conditions is the first step in CFD. For problems in Fluid Mechanics and Heat Transfer, it is needed to create or extract the geometry for the domain where the fluid flow is expected to occur. Many CAD packages with a graphical user interface for creation of geometry are available today.

2.1.2 Preprocessing

Once the geometry has been created, the next step is discretizing the domain i.e. dividing the domain into a number of elements of same or different nature. The preprocessing step is one of the most important and probably the most time consuming step in the CFD process. The accuracy of the solution heavily depends on the quality of the mesh generated. Generation of mesh can be different in different areas of the solution domain. For example, one may need a finer mesh close to the wall boundaries of the geometry to capture the gradients existing in the boundary layer there. The type of mesh to be generated also depends on the complexity of the geometry available, computer resources, nature of flow and time availability. Structured grids are usually created when the nature and direction of flow is known beforehand and geometry is fairly simple. However recent research in grid generation has given rise to the use of unstructured grids which give a fairly accurate solution and save a lot of time when

compared with creation of structured grids. After evaluation of these parameters, the decision to create the type of grid depends on the intuition, experience and skill of the user.

2.1.3 Problem setup

After the grid is generated, it is setup according to the initial and boundary conditions. Precise identification of the boundary and initial conditions and their appropriate numerical application is very important to get a realistic solution. Material selection and implementation of its properties is done in the setup. The solution method or algorithm, appropriate models for the methods and level of accuracy required by defining the residual convergence criteria while solving the flow equations are also decided in this step.

2.1.4 Solution

The solution for the governing equations is then calculated at different grid points or elements using the chosen method. For obtaining a CFD solution, one of finite difference, finite volume or finite element methods is used. Use of the finite element method is more popular in structural problems and needs further research and development for solving flow problems. The Finite difference method involves use of a structured grid with uniform or non-uniform spacing and use of numerical methods by marching either in space or time to obtain numerical values at each grid point. The Finite volume method consists of discretizing the domain into several well defined volumes or cells. The volume averaged values of the conserved variables are obtained using this method. The mass, momentum and energy equations are conserved in this method. This method also facilitates the use of an unstructured grid which is useful in case of complex

geometries. The finite volume method is therefore popular among fluid dynamicists and engineers in general.

2.1.5 Post processing

The last step of the CFD process is post processing where the results are analyzed using graphs, contour plots, etc. The values of the parameters to be analyzed are extracted.

A lot of commercial post-processing packages are available to view results for analysis.

2.2 Governing Equations

In CFD, the Navier Stokes equations which govern all problems related to Fluid Mechanics and Heat Transfer are solved numerically. The Navier Stokes equations are 3D coupled set of partial differential equations. They are derived on the basis of laws of physics dictating conservation of mass, momentum and energy.

2.2.1 Continuity equation

The continuity equation is derived from the law that mass of an isolated system is conserved. In this study, steady state analysis of incompressible flow without considering gravity effects is considered. Therefore, the non dimensional form of the 3D incompressible continuity equation with no time variants is given in the following form

$$\frac{\partial(u^*)}{\partial x^*} + \frac{\partial(v^*)}{\partial y^*} + \frac{\partial(w^*)}{\partial z^*} = 0$$

2.2.2 Momentum equation

The momentum equation is derived on the basis of the principle of conservation of momentum which states that the total momentum on a volume should be conserved. So, the dimensionless 3D steady incompressible momentum equation is given in the following form.

$$u^* \frac{\partial u^*}{\partial x^*} + v^* \frac{\partial u^*}{\partial y^*} + w^* \frac{\partial u^*}{\partial z^*} + \frac{\partial P^*}{\partial x^*} = \frac{1}{Re} \left(\frac{\partial^2 u^*}{\partial x^{*2}} + \frac{\partial^2 u^*}{\partial y^{*2}} + \frac{\partial^2 u^*}{\partial z^{*2}} \right)$$

$$u^* \frac{\partial v^*}{\partial x^*} + v^* \frac{\partial v^*}{\partial y^*} + w^* \frac{\partial v^*}{\partial z^*} + \frac{\partial P^*}{\partial y^*} = \frac{1}{Re} \left(\frac{\partial^2 v^*}{\partial x^{*2}} + \frac{\partial^2 v^*}{\partial y^{*2}} + \frac{\partial^2 v^*}{\partial z^{*2}} \right)$$

$$u^* \frac{\partial w^*}{\partial x^*} + v^* \frac{\partial w^*}{\partial y^*} + w^* \frac{\partial w^*}{\partial z^*} + \frac{\partial P^*}{\partial z^*} = \frac{1}{Re} \left(\frac{\partial^2 w^*}{\partial x^{*2}} + \frac{\partial^2 w^*}{\partial y^{*2}} + \frac{\partial^2 w^*}{\partial z^{*2}} \right)$$

2.2.3 Energy equation

The energy equation is derived on the basis of the law of the conservation of energy which states that the total amount of energy of a volume is conserved over time. The dimensionless 3D steady incompressible energy equation is given in the following form.

$$\frac{\partial (u^* T^*)}{\partial x^*} + \frac{\partial (v^* T^*)}{\partial y^*} + \frac{\partial (w^* T^*)}{\partial z^*} = \frac{1}{Re\, Pr} \left[\frac{\partial^2 T^*}{\partial x^{*2}} + \frac{\partial^2 T^*}{\partial y^{*2}} + \frac{\partial^2 T^*}{\partial z^{*2}} \right]$$

Chapter 3

Computational Setup

The problem setup, meshing of the fluid domain and solution strategy are described in this chapter. Commercial CAE packages were used for different steps of the CFD process to obtain the solution. The flow area inside the channel was modeled, meshed and setup for solution with the use of these CAE packages.

3.1 Modeling of the computational domain

The fluid flow area inside the channel was modeled using the commercial CAD software Creo. To model dimples inside the channel, bumps were created on the base of the channel with 2 different array geometries. An inlet section with length same as the heated bottom wall was created to ensure fully developed flow conditions while an outlet section with twice the length of the heated section. The heated part of the channel was 64×22.5×2.5 cm (L×B× H) in dimensions. The channel was modeled with two different dimple array geometries on the bottom wall: A staggered array of 21×7 dimples and a 19×4 inline array. The staggered array had 4 and 3 dimples in alternating rows while the inline array had 4 dimples in each row. The dimple print diameter to depth ratio (δ/D) was kept at 0.2. The dimple print diameter was kept at 2.5 cm. According to the analysis and microelectronic sink redesign by Silva et al [28], effort was taken to increase the surface area between dimples to boost the heat transfer enhancements. A distance of 1.2 D was kept between consecutive rows and columns of the staggered array. The channel height was kept at 2.5 cm making the H/D ratio equal to 1. The geometry of the staggered and inline dimpled array on the bottom wall of the channel is shown in Figure 3-1 and Figure 3-2. The isometric view of the inline dimpled array channel is shown in Figure 3-3 while Figure 3-4 shows the specifications of single dimple.

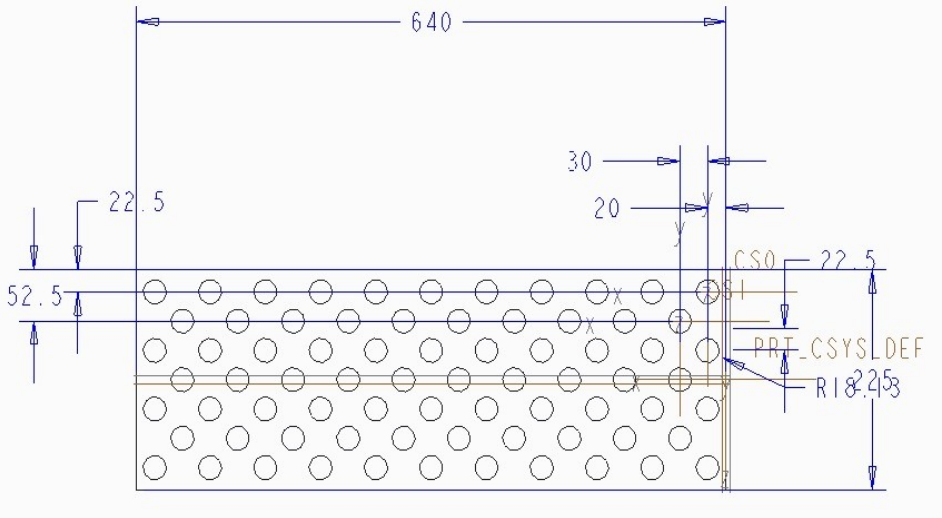

Figure 3-1 Staggered array of dimples of the bottom wall of the channel

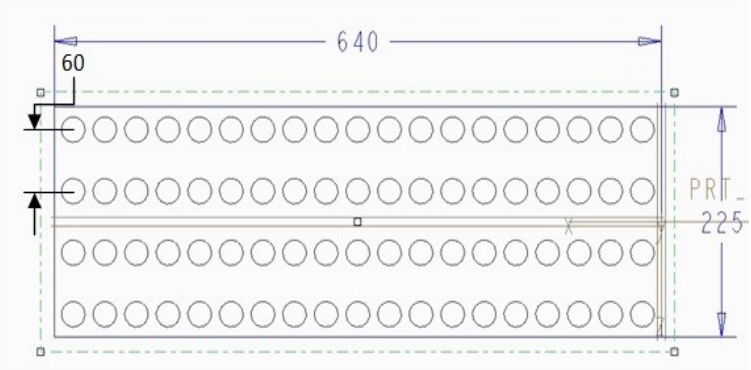

Figure 3-2 Inline dimpled array on the bottom wall of the channel

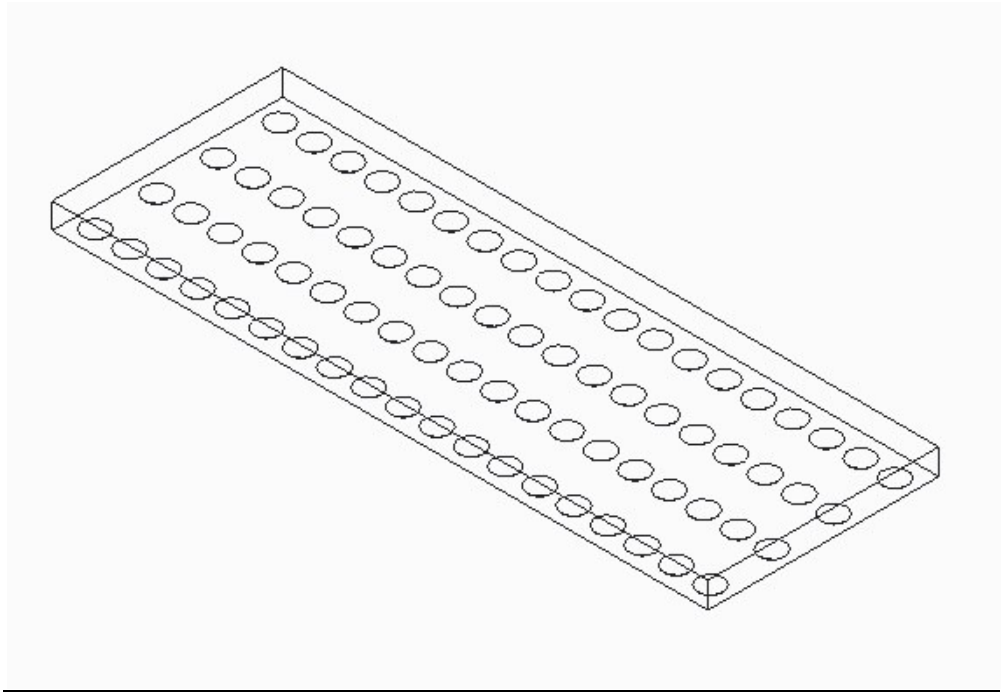

Figure 3-3 Isometric view of the inline dimpled channel

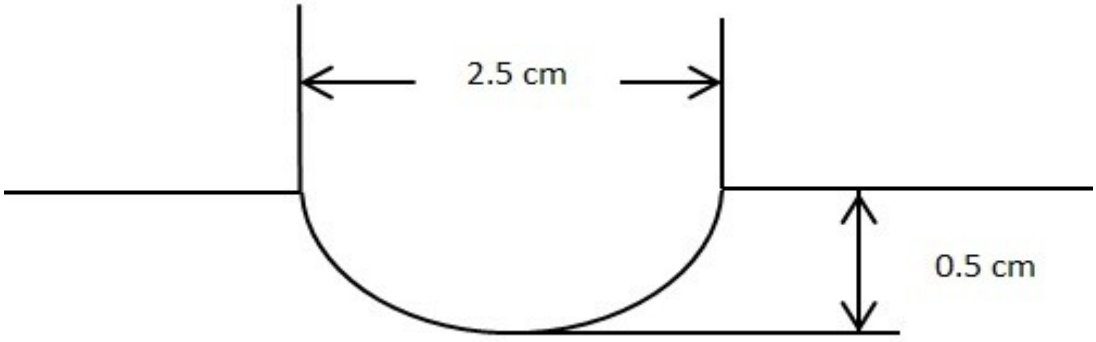

Figure 3-4 Specifications of dimple on the bottom wall of the channel

3.2 Grid generation

Ansys Workbench was used for meshing the computational domain. A mixed tetrahedral/prism mesh was generated. Prisms were used in the inflation layer to capture the high gradients near the wall of the channel. The first layer height was set to 5e-4 in the inflation layer with a growth rate of 1.2. The total numbers of layers were set to 5. The relevance was set to fine to ensure smooth transition of the tetrahedrons from the inflation layer. The proximity and curvature advanced sizing function was used. The meshed domain is shown in Figure 3-5

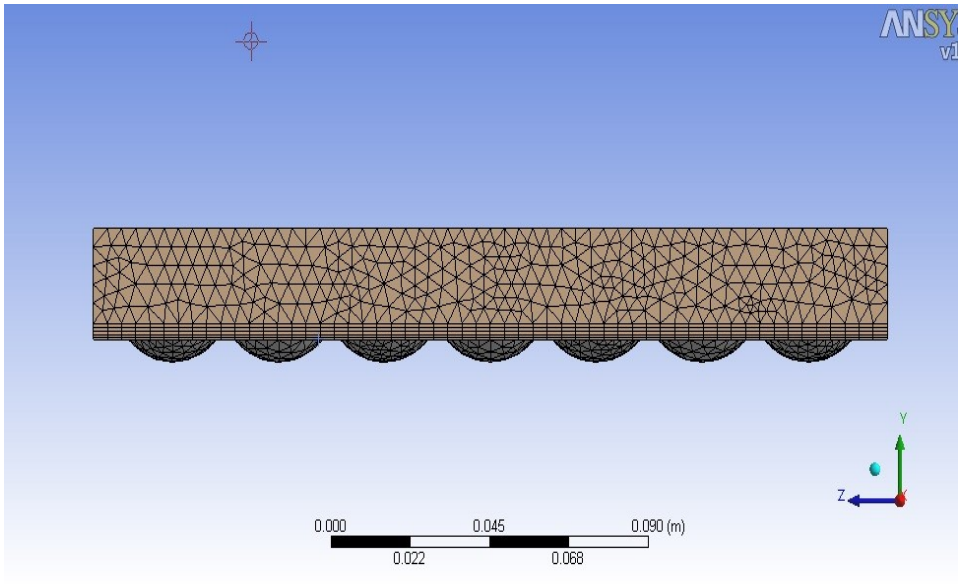

Figure 3-5 Tetehedral mesh with inflation on the dimpled channel

3.2.1 Grid dependency study

A grid dependency study was carried out to obtain grid independent solutions. In a grid dependency study, a family of grids is created by refining the previous grid and the solution is calculated until the solution stops changing. The grids selected for the geometries are given in Table 3-1

Table 3-1 Grids selected for various geometries

Geometry	Number of elements
Smooth Channel	2101497
Staggered Array	2149841
Inline Array	2189013

3.3 Solution setup

The commercial CFD software Fluent 12.0.16 was used for the computational solution. The mesh was read in to Fluent and setup for solution. Fluent uses the finite volume method to solve for the governing equations. Fluent has good capabilities of solving unstructured meshes even for complex geometries. Due to lack of need for coordinate transformations in finite volume method used by Fluent, it is popular for solution of Fluid mechanics and Heat Transfer problems and hence is selected for this study.

3.3.1 Solver

The pressure based segregated implicit solver was selected for the solution. The pressure based solver is typically used for low speed incompressible flows and hence was selected for the present study of laminar airflows on dimpled surface. In this solver, the momentum equation is used to obtain the velocity field while the pressure field is obtained from the pressure correction equation which is derived by manipulating the continuity and momentum equations. The energy equation was also solved as it was desired to observe thermal effects.

3.3.2 Material properties and flow conditions

Air was the fluid material selected for flow inside the channel. The laminar viscous model was used to model the flow conditions. The material properties of air are given in the table

Table 3-2 Material Properties

Property	Value
Thermal Conductivity	0.0242 w/m-k
Density	1.225 kg/m^3
Viscosity	1.7894e-5

3.3.3 Boundary conditions

Correct numerical application of boundary conditions is necessary for CFD solution accuracy and the problem to be modeled more realistically. The following boundary conditions were applied to the mesh.

3.3.3.1 Velocity Inlet

The velocity was calculated from the Reynolds number based on the Hydraulic diameter of the channel. The Reynolds number is a dimensionless number which is given as

$$\mathrm{Re} = \frac{\rho v \mathrm{H_d}}{\mu},$$

The hydraulic diameter H_d is given as

$$\mathrm{H_d} = \frac{4 \times \mathrm{A}}{\mathrm{Pe}}$$

The calculated velocity from the Reynolds number was applied to the inlet of the channel. The applied velocity was used to calculate mass flow and momentum flux with

the magnitude of velocity normal to the boundary only used for calculation of mass flow rate. The temperature at the inlet, T_{in} was set at 300 K

3.3.3.2 Pressure Outlet

The outlet of the channel was assigned the zero gauge pressure outlet condition which is the default in Fluent. All other values are extrapolated from the interior of the domain.

3.3.3.3 Wall and thermal boundary conditions

The bottom wall of the channel where the dimpled array is present was assigned constant temperature boundary condition. A temperature, T_{wall}, of 375 K was assigned to this wall to indicate heating at the bottom wall of the test surface while all other walls were assigned adiabatic boundary condition. A no slip boundary condition was assigned to all walls that is the velocity of the flow at the wall is zero.

3.3.4 Solution Methods and Controls

In this step of Fluent, different solution discretization methods and controls for residual monitors and under relaxation factors can be set.

3.3.4.1 Pressure Velocity Coupling and Discretization scheme

The SIMPLE method was chosen for the pressure velocity coupling. In the SIMPLE algorithm, approximation of the velocity field is obtained from the momentum equation while the pressure distribution from the previous iteration is used to calculate the pressure gradient term [26]. The new pressure distribution is obtained by solving the

pressure equation formulated while velocities are corrected and a new conservative set of fluxes is calculated [26].

The second order upwind spatial discretization scheme was chosen to solve the momentum and energy equations. The second order discretizations were chosen as they give higher order accuracy.

3.3.4.2 Under relaxation factors

The default under relaxation factors of 0.3 for pressure, 1 for density 0.7 for momentum and 1 for energy were used. Selections of these under relaxation factors helped in reducing the numerical dissipation errors and achieve faster convergence.

3.3.4.3 Residuals and surface integrals monitor

All residuals were set to 1e-3 with the exception of residuals for energy equation which were set to 1e-6 for convergence. The heated surface average Nusselt number and heat transfer coefficients monitors were also created. The surface averaged Nusselt number and surface averaged heat transfer coefficient plots flattened out before convergence was reached.

3.3.4.4 Solution Initialization and calculation

The solution was then initialized with all values computed from the inlet face. The solution was then calculated until the surface monitors and the residuals flattened out to the set level of accuracy.

Chapter 4

Results and Discussion

The results of heat transfer characteristics are presented for laminar airflows. Two different dimple array geometries in case of dimpled channel were compared with the smooth channel. Several parameters were used for the purpose of heat transfer characteristics comparison. The average surface Nusselt number, average heat transfer coefficient and thermal performance parameter based on the Nusselt number ratio and pressure drop across the channel were used for heat transfer characteristics comparison.

4.1 Nusselt number

Nusselt number is a dimensionless number which is a ratio of convective to conductive heat transfer normal to the boundary at a surface within a fluid. Thus, it measures the performance of convective heat transfer over conductive heat transfer.

For a surface within a flow, the Nusselt number is given by

$$\mathrm{Nu} = \frac{\mathrm{hL}}{\mathrm{k}}$$

In this study, the surface averaged Nusselt number at the interface of the heated section is compared for all the three channels: The smooth channel, the channel with the staggered dimple array and the channel with the inline dimpled array. The contour plots of Nusselt numbers at the interface are shown and compared. The surface averaged Nusselt numbers for the smooth channel interface $\overline{\mathrm{Nu}_0}$ are taken as baseline data for comparison. The Nusselt number ratio $\overline{\mathrm{Nu}} / \overline{\mathrm{Nu}_0}$ comparing surface averaged Nusselt number of dimpled geometry interface and surface averaged Nusselt number of smooth channel are plotted against the Reynolds number (based on hydraulic diameter) range studied.

The $\overline{Nu} / \overline{Nu_0}$ values for the staggered dimpled array geometry and the inline dimpled array geometry are plotted for the Reynolds number ranging from 750 to 1500 in Figure 4-1. It can be seen that the $\overline{Nu} / \overline{Nu_0}$ values increase with increasing Reynolds number for both the inline array geometry and the staggered array geometry. It can also be seen that the staggered array geometry has higher $\overline{Nu} / \overline{Nu_0}$ values than the inline array geometry for a corresponding Reynolds number. However the Nusselt number values for both the dimpled geometries were greater than the smooth channel geometry irrespective of Reynolds number. When compared with the available literature for use of dimples in the turbulent flow regime, it can be seen that the $\overline{Nu} / \overline{Nu_0}$ ratios have much lower values for the laminar flow regime studied suggesting lower levels of heat transfer augmentation for the low Reynolds number range.

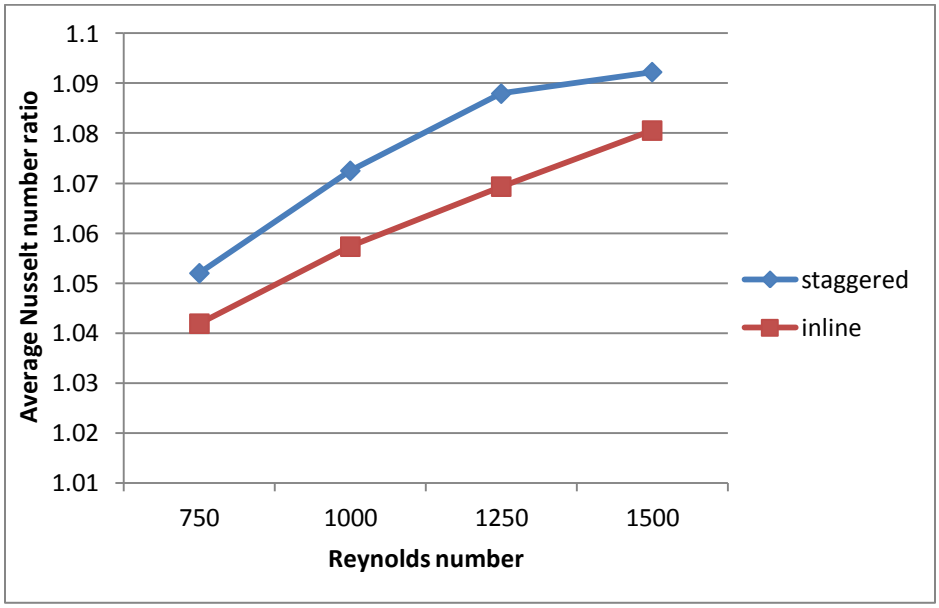

Figure 4-1 Nusselt number ratio comparison for staggered and inline array geometries vs Reynolds number

The Nusselt number contour plots for the staggered and inline array geometries for Reynolds number 750 and 1000 are shown in Figure 4-2 to Figure 4-9.

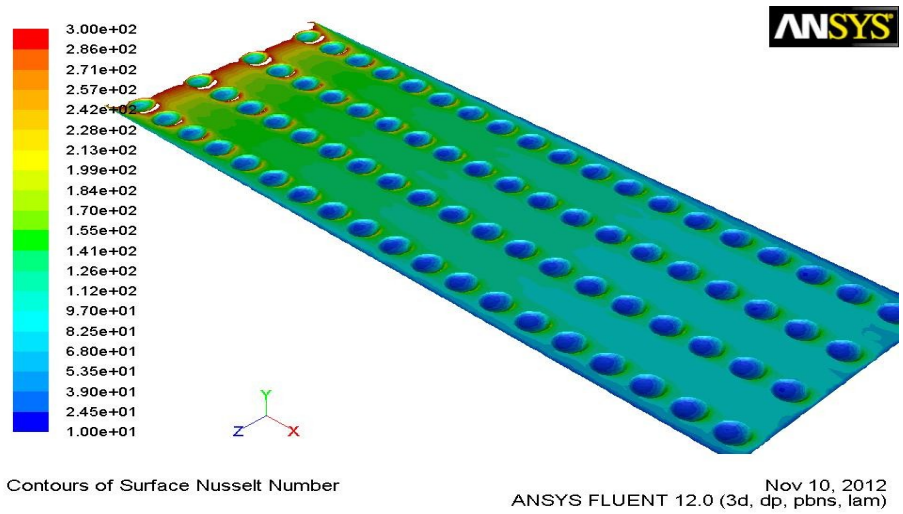

Figure 4-2 Nusselt number contour plot for inline dimpled array geometry at Reynolds number 750

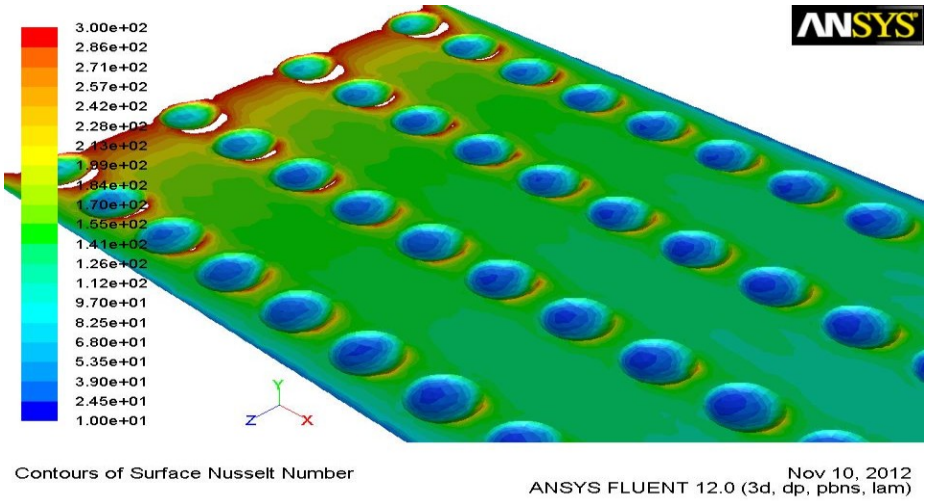

Figure 4-3 Nuselt number contour plot at upstream location for inline dimpled array at Reynolds number 750

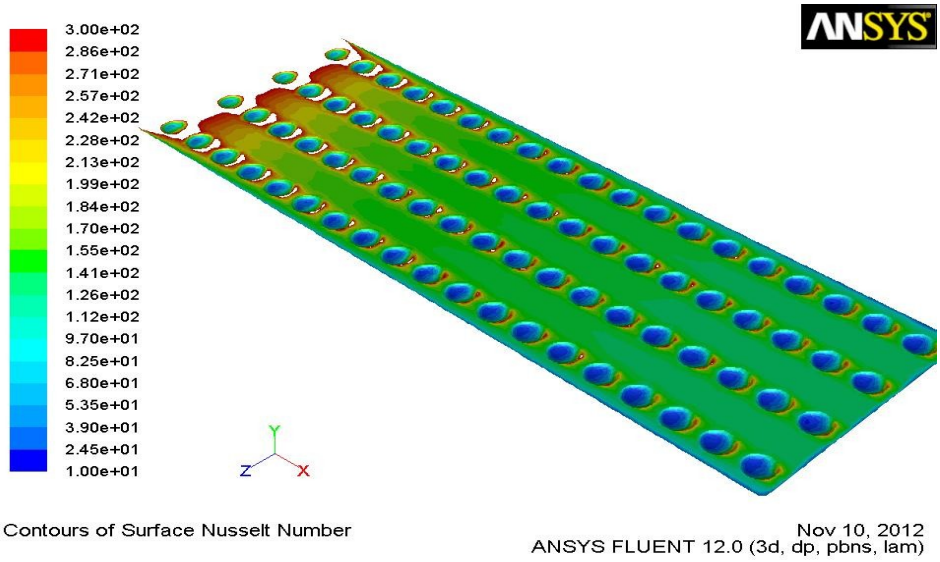

Figure 4-4 Nusselt number contour plot for inline dimpled array geometry at Reynolds number 1500

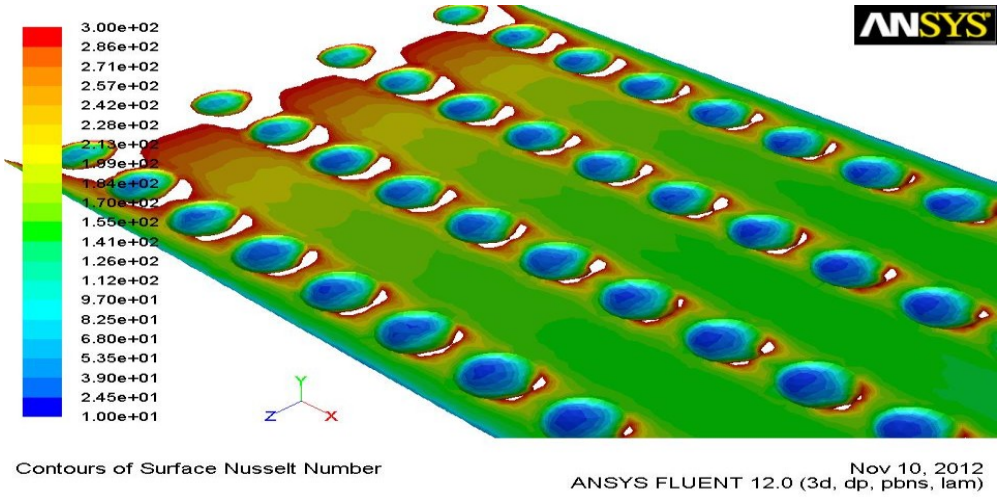

Figure 4-5 Nusselt number plot at the upstream location for inline dimpled geometry at Reynolds number 1500

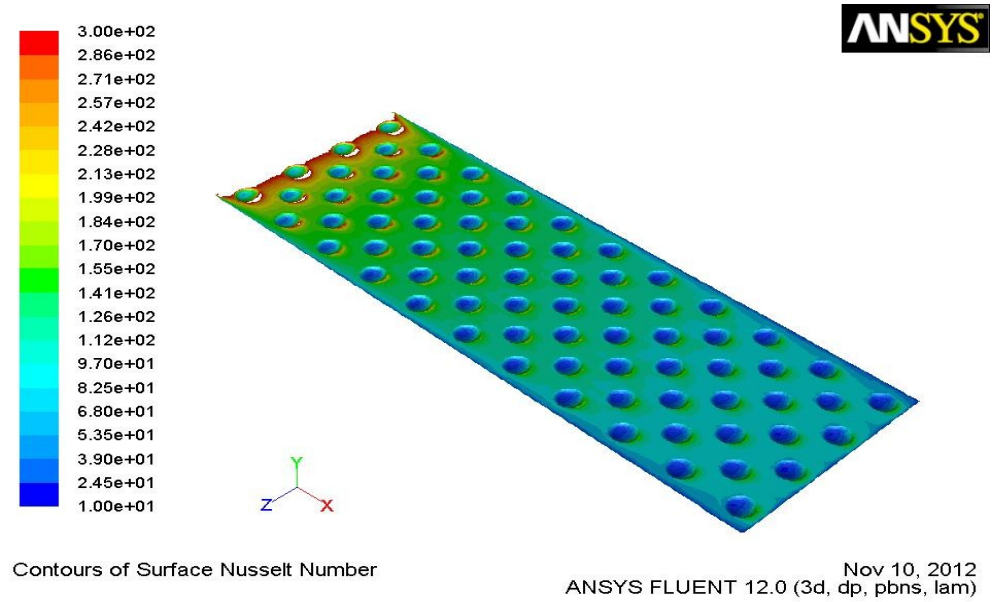

Figure 4-6 Nusselt number plot for staggered dimpled array geometry at Reynolds number 750

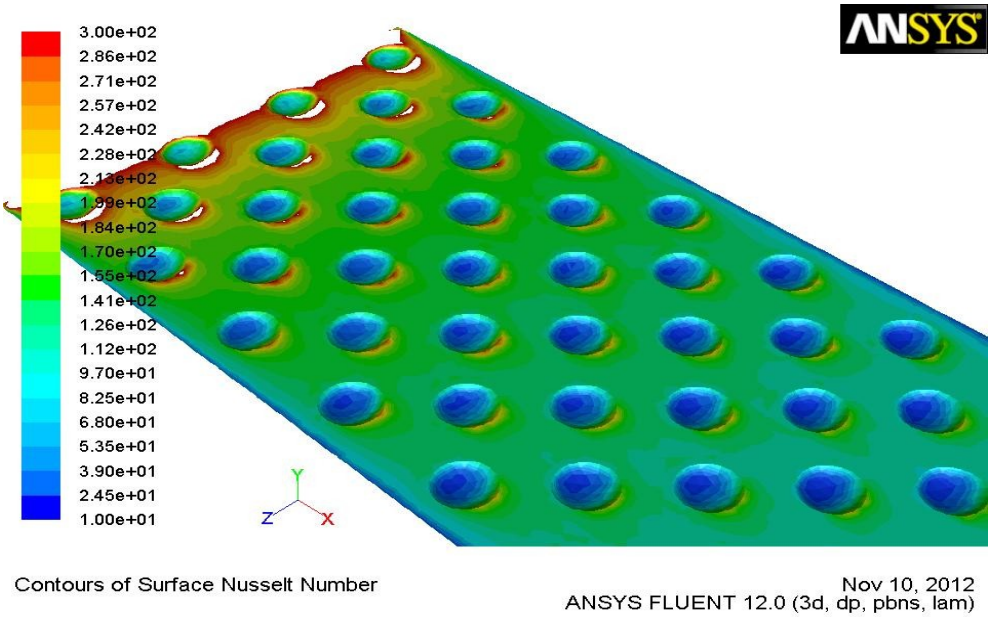

Figure 4-7 Nusselt number plot at the upstream location for staggered dimpled array geometry at Reynolds number 750

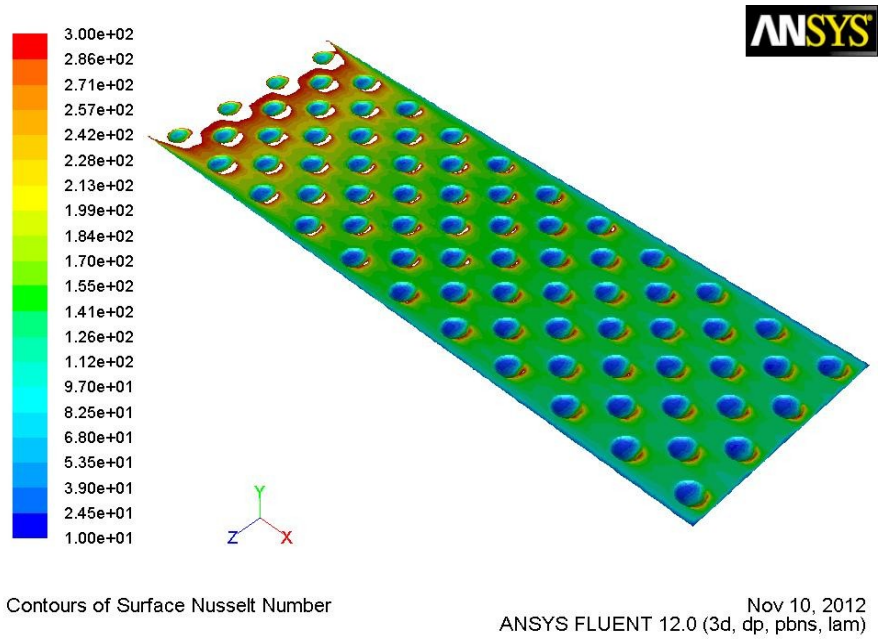

Figure 4-8 Nusselt number plot for staggered dimpled array geometry at Reynolds number 1500

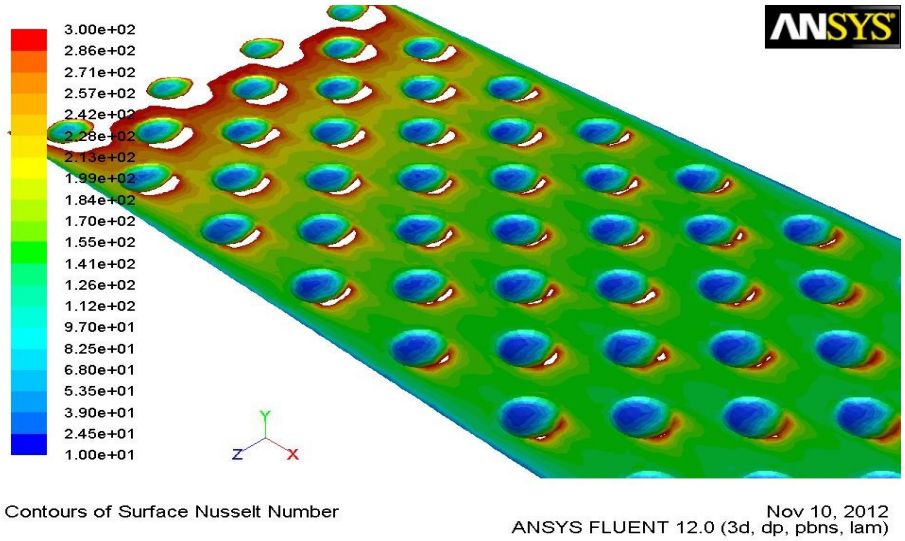

Figure 4-9 Nusselt number plot at the upstream location for staggered dimpled array geometry geometry at Reynolds number 1500

In the Nusselt number contour plots, the flow direction is from left to right. In all of the plots highlighting the upstream area with high Nusselt number variation, it can be seen that the surface Nusselt numbers are maximum near the downstream rim of the dimple and on the flat area downstream of the dimple. The upstream area of the dimple and the area deep upstream inside the dimple and have the lowest Nusselt number values in both the geometries. This shows that the flat area downstream of the dimple is vital for convective heat transfer signifying the design of the model having a distance of 1.2 X D between consecutive rows and columns of the staggered array.

It can also be seen that the Nusselt number variation is high in the upstream area of the dimpled surface while it reduces downstream. For the case of Reynolds number 750, the variation in Nusselt number on the surface stops higher upstream than in the case of Reynolds number 1500 for both geometries. The halt in Nusselt number variation upstream suggests that higher thermal performance might have been achieved without using the dimples in the downstream area where the Nusselt number contour plot shows no variation and follows a consistent pattern. The dimples in this area majorly contribute to skin friction drag and hence hydraulic losses and not so much in heat transfer augmentation thus lowering the overall thermal performance. As the location where the Nusselt number variation stops moves further downstream with increase in Reynolds number, the geometry of dimples and the number of dimples used might work much better with respect to heat transfer enhancement for the high Reynolds number flow regime.

In general, slightly higher Nusselt number values for the dimpled geometries over the smooth channel indicate heat transfer enhancement. In the next section, the comparison of convective heat transfer coefficient is shown as heat transfer characteristic comparison.

4.2 Heat transfer coefficient

The heat transfer coefficient in heat transfer is a measure of calculating the convective heat transfer. It is given in the following form.

$$h = \frac{Q}{A_t \,.\, \Delta T}$$

The heat transfer coefficient can be calculated from the thermal conductivity of the working fluid and the Nusselt number. Like the Nusselt number comparisons, the average heat transfer coefficient ratios with respect to the baseline data at the interface are plotted for both the staggered dimpled array geometry and inline dimpled array geometry. The $\bar{h}/\overline{h_0}$ plot for the two geometries is shown in Figure 4-10

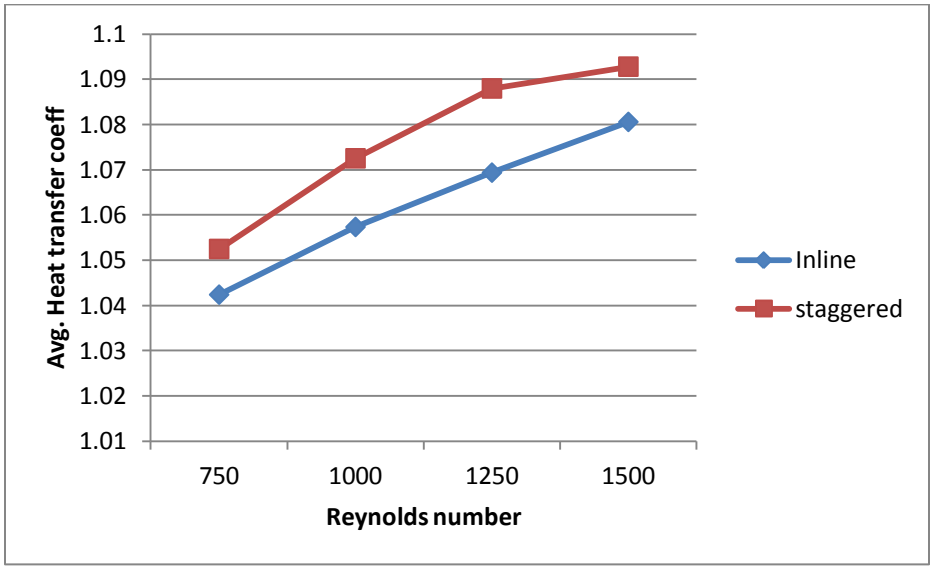

Figure 4-10 Plot of h/ho values for inline dimpled array and staggered dimpled array geometry vs Reynolds number

The $\bar{h}/\overline{h_0}$ plots show the same pattern as the $\overline{Nu} / \overline{Nu_0}$ plots with increasing $\bar{h}/\overline{h_0}$ ratios with increasing Reynolds number. Also, the $\bar{h}/\overline{h_0}$ ratios for the staggered

array case are slightly higher than the inline dimpled array case for all Reynolds numbers.

The heat transfer coefficient contour plots for the two geometries are shown for the Reynolds number case of 1500 in Figure 4-11 and Figure 4-12. The plots show the same trend as the Nusselt number contour plots with the highest heat transfer coefficients appearing at the downstream rim of each dimple and on the flat area downstream of the dimple signifying importance of that area in convective heat transfer enhancement. Also, the heat transfer coefficient variation in the contour plot halts upstream suggesting lower number of dimples spread over the area might have given better thermal performance for laminar airflows.

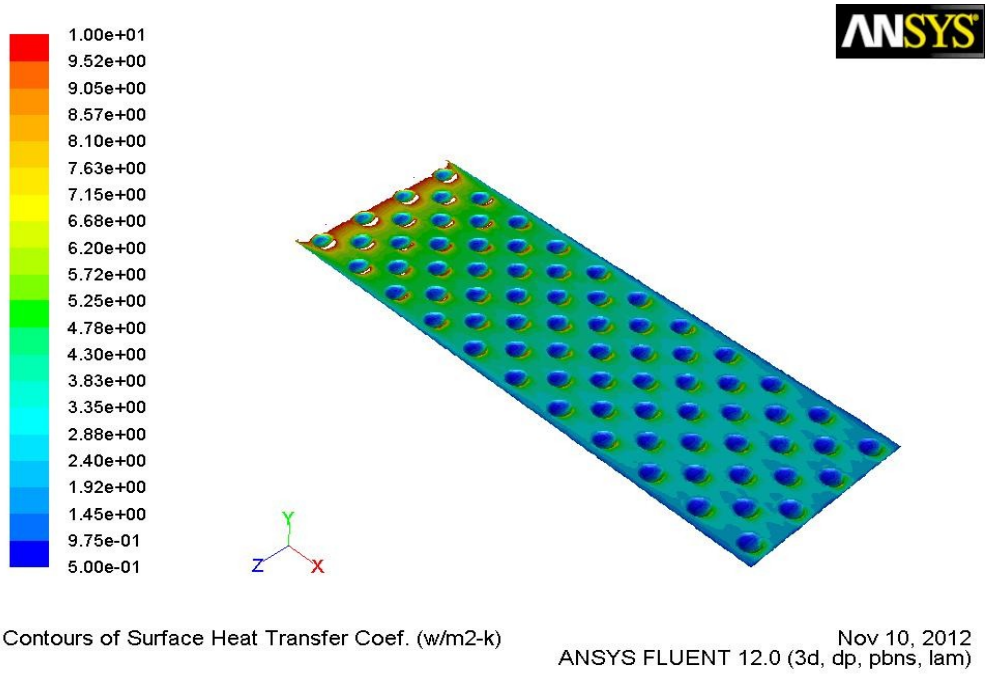

Figure 4-11 Heat transfer coefficient contour plot for staggered dimpled array geometry for Reynolds number 1500

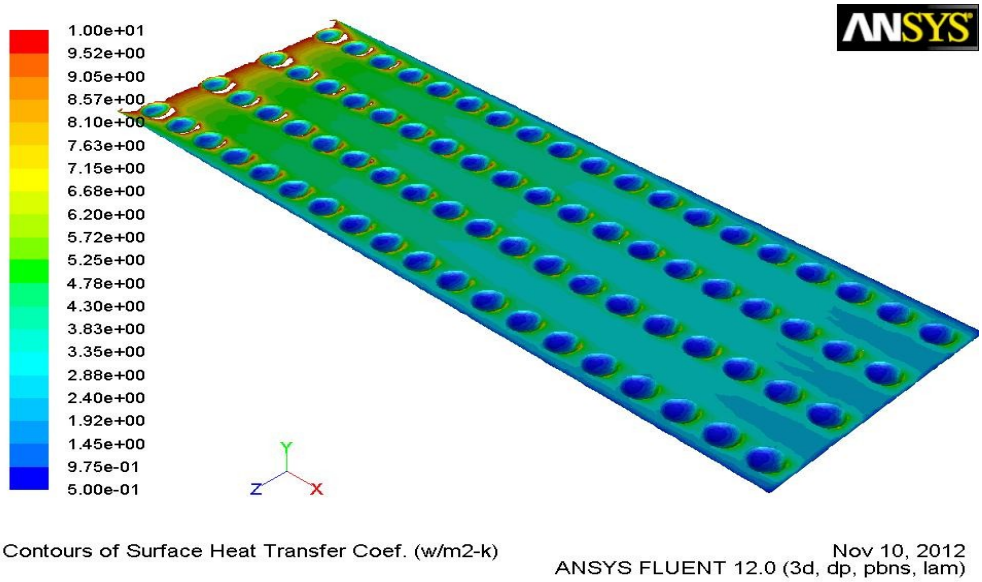

Figure 4-12 Heat transfer coefficient contour plot for inline dimpled array geometry at Reynolds number 1500

The use of dimpled surface thus gives augmented values of heat transfer coefficient and Nusselt number at the interface. However, the use of dimples also increases skin friction drag increasing pressure losses. These pressure losses caused by increase in friction factors are shown in the next section.

4.3 Friction factors

As the use of dimpled surfaces for heat transfer enhancement is known to increase hydraulic losses, the friction factors for the two dimpled geometries are compared with the smooth channel. The friction factor is a dimensionless quantity in the Darcy-Weisbach equation which is used to calculate pressure loss due to friction in pipes, channels and ducts. The Darcy- Weisbach equation is given in the following form.

$$h_f = f_D \cdot \frac{L}{H_d} \cdot \frac{v^2}{2g}$$

In terms of pressure loss, the Darcy- Weisbach equation can be written as

$$\Delta p = f_D \cdot \frac{L}{H_d} \cdot \frac{\rho v^2}{2}$$

The Δp values are calculated directly from Fluent as the difference between the inlet and outlet pressures of the channel whereas the diameter of the pipe is replaced by the hydraulic diameter of the channel. The friction factor values are calculated and the friction factor ratios with respect to the baseline data for staggered dimpled array geometry and the inline dimpled array geometry are plotted. The f/f_0 values for the two geometries at the Reynolds numbers studied are plotted in Figure 4-13

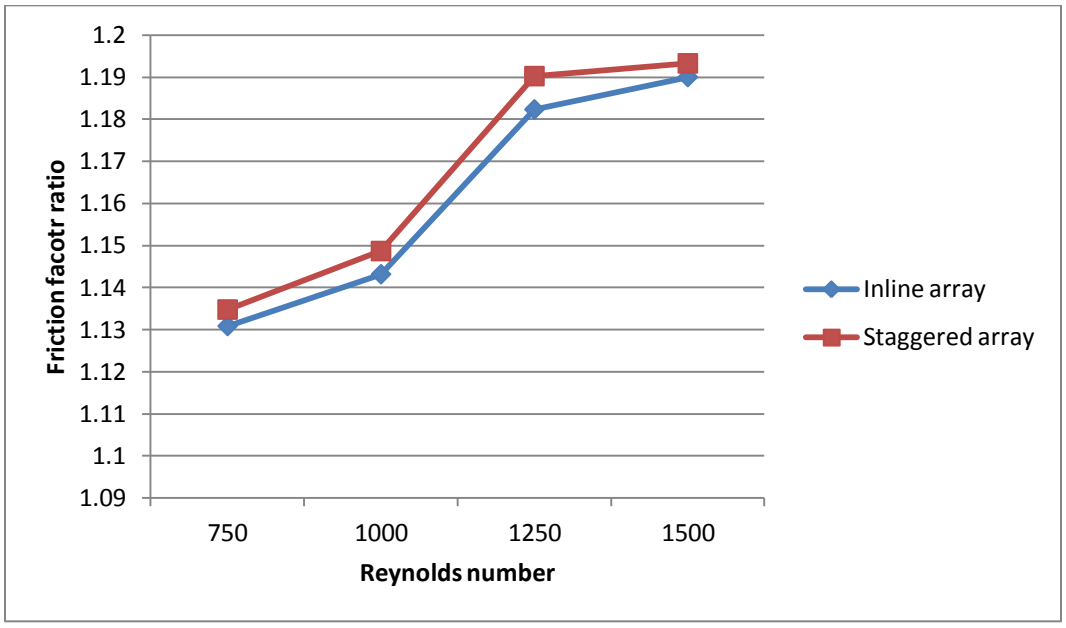

Figure 4-13 Plot of friction factor ratios for staggered dimpled array and inline dimpled array geometries vs Reynolds number

It can be seen from the plot that dimples do increase friction factors over smooth channels. The friction factor ratios for the staggered dimpled array geometry are more than the inline dimpled array geometry. The friction factors and the pressure drop have a major impact on the thermal performance of the channel. The pressure loss also has to be accounted along with the convective heat transfer coefficient augmentation. The performance of a heat sink can be judged only by taking into account the hydraulic losses and whether the heat transfer coefficient augmentations are worth the hydraulic loss incurred. This can be evaluated by calculating the thermal performance factor which is discussed in the next section.

4.4 Thermal performance factor

As discussed in the literature and from elementary aerodynamics, the use of dimples does not introduce form drag unlike protruding objects. However, the use of dimples gives rise to increase in skin friction drag and hence dimples cannot be used for drag reduction in channels. As shown in the previous section, dimples increase the friction factor of the channel over the smooth channel and thereby increase the pressure loss of the channel as given by the Darcy- Weisbach equation. For an efficient heat sink, the thermal performance factor has to be greater than 1. For turbulent airflows, the heat transfer enhancements as much as 200 % have been found in the available in the literature.

The thermal performance factor is calculated using the following equation

$$\mathrm{TP} = (\mathrm{Nu}/\mathrm{Nu}_0)(\mathrm{f}/\mathrm{f}_0)^{-1/3}$$

This factor gives the thermal performance per unit pumping power by the dimpled surface in comparison to the thermal performance per unit pumping power in case of the smooth channel.

The thermal performance factor for the staggered dimpled array and inline dimpled array geometry for the Reynolds number range studied are plotted in Figure 4-14

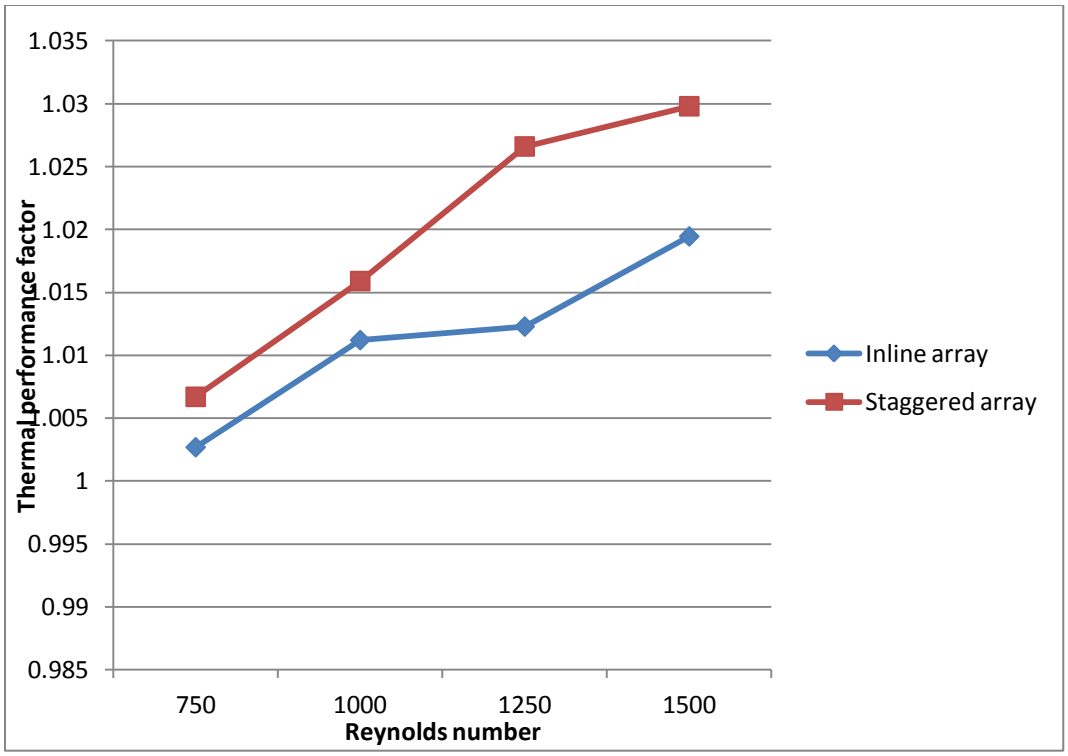

Figure 4-14 Plot of thermal performance factors for the staggered dimpled array and inline dimpled array vs Reynolds number

The plot shows that the thermal performance increases with increasing Reynolds number for both geometries. Again, the thermal performance factor for the staggered geometry is higher than the inline geometry at all Reynolds numbers. In the Reynolds number range from 1000 to 1250, the thermal performance factor for the inline dimpled array geometry did not rise as much as the one for the staggered dimpled array geometry did. This was mainly due to substantial increase in $\overline{\mathrm{Nu}} / \overline{\mathrm{Nu}_0}$ value for the staggered dimpled array geometry over the inline dimpled array geometry. In general, the thermal performance factor followed the same trend of increasing with increase in Reynolds as other parameters compared before.

4.5 Flow structure and velocity vectors

The flow structure of the airflow over the dimpled surface was studied by observing the velocity vectors. The post processing capability of Fluent was used to view the velocity vectors. To analyze the flow, the vectors were observed from the spanwise and streamwise direction of the channel. This was done to investigate the presence of any secondary flows. From elementary fluid mechanics, a secondary flow is a minor flow superimposed on the primary flow and which is not predicted by simple analytical techniques. The velocity vectors showing the primary flow following the contour of the dimple for both the staggered dimpled array geometry and inline dimpled array geometry for Reynolds numbers 1000 and 1500 are shown in Figure 4-15 to Figure 4-18.

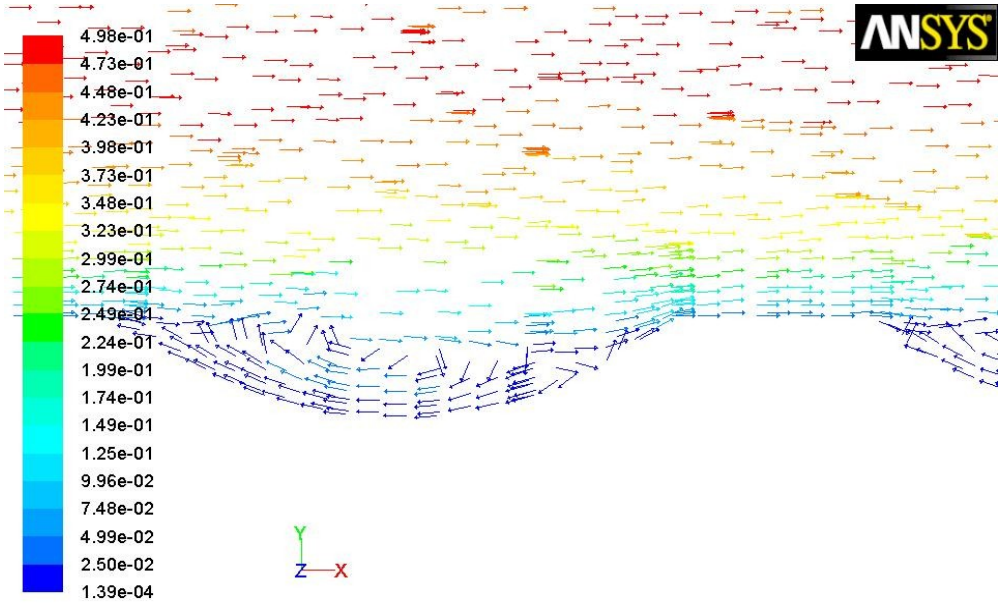

Figure 4-15 Velocity vectors for inline dimpled array for Reynolds number 1000

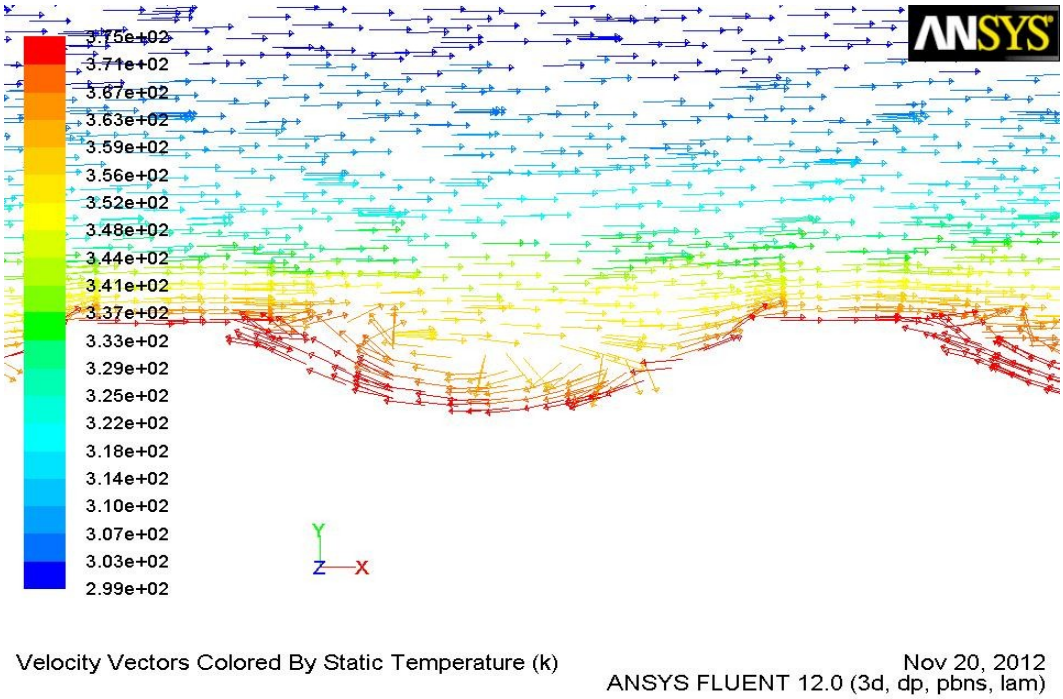

Figure 4-16 Velocity vectors for inline dimpled array for Reynolds number 1500

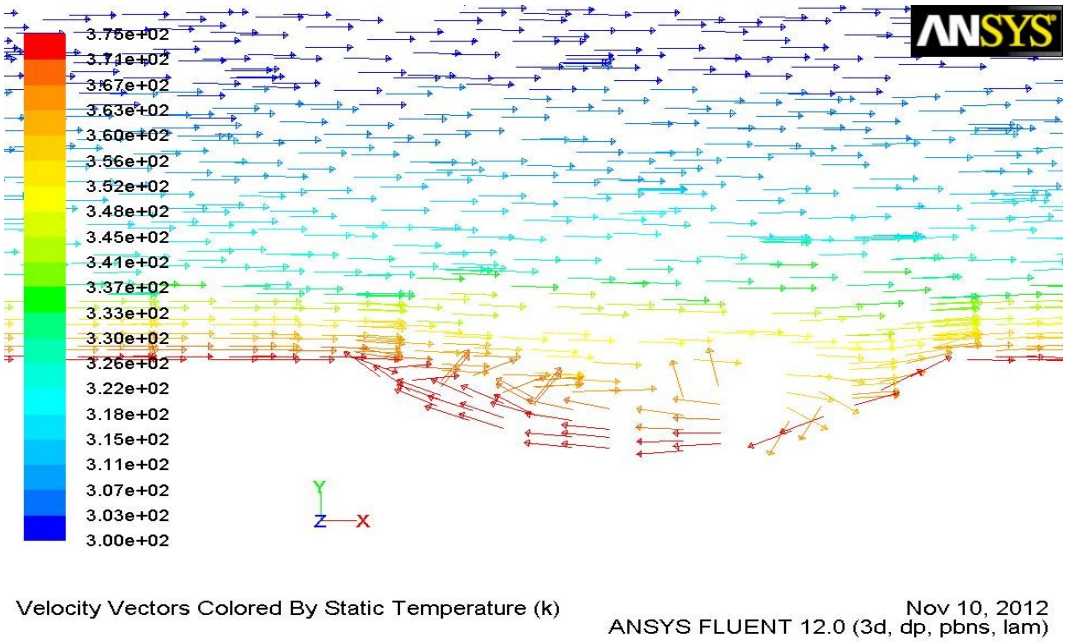

Figure 4-17 Velocity vectors for staggered dimpled array for Reynolds number 1000

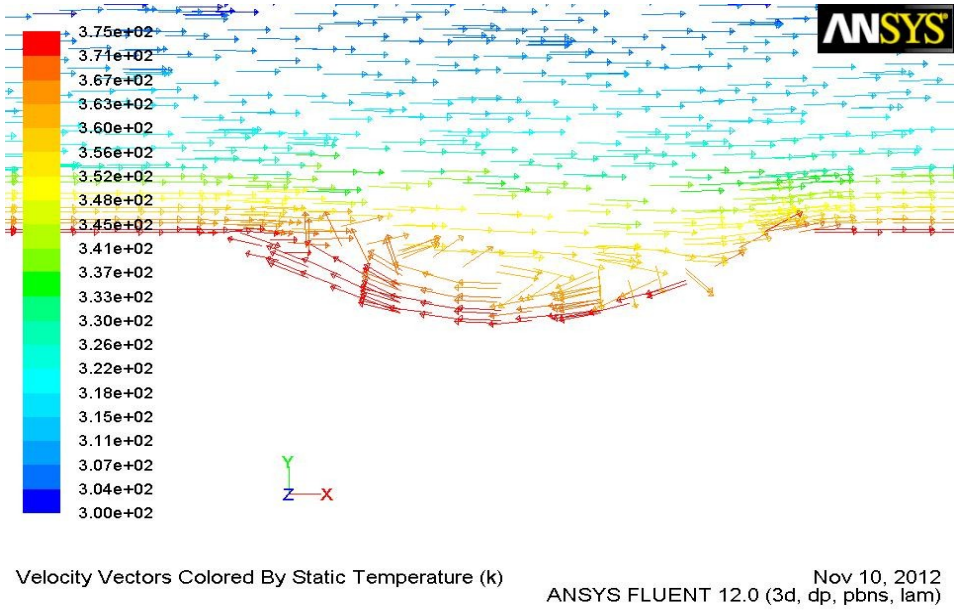

Figure 4-18 Velocity vectors for staggered dimpled array for Reynolds number 1500

It can be seen from the velocity vectors for the two geometries considered that circulation regions exist in case of dimples for the Reynolds numbers observed. The circulations are observed in the upstream area of the dimple as well as deep inside the dimple. It can also be seen from the velocity vectors that the circulations get stronger as the Reynolds number increases. It can also be seen that the flow reattaches on the flat area downstream of the dimple. This is responsible for enhancing the convective heat transfer in that area. However, the recirculation region inside of the dimple traps the flow there and reduces convective heat transfer in that region which is also evident from the Nusselt number and heat transfer coefficient contour plots.

The secondary flows for the two geometries at Reynolds number 1000 and 1500 are shown in Figure 4-19 to Figure 4-22.

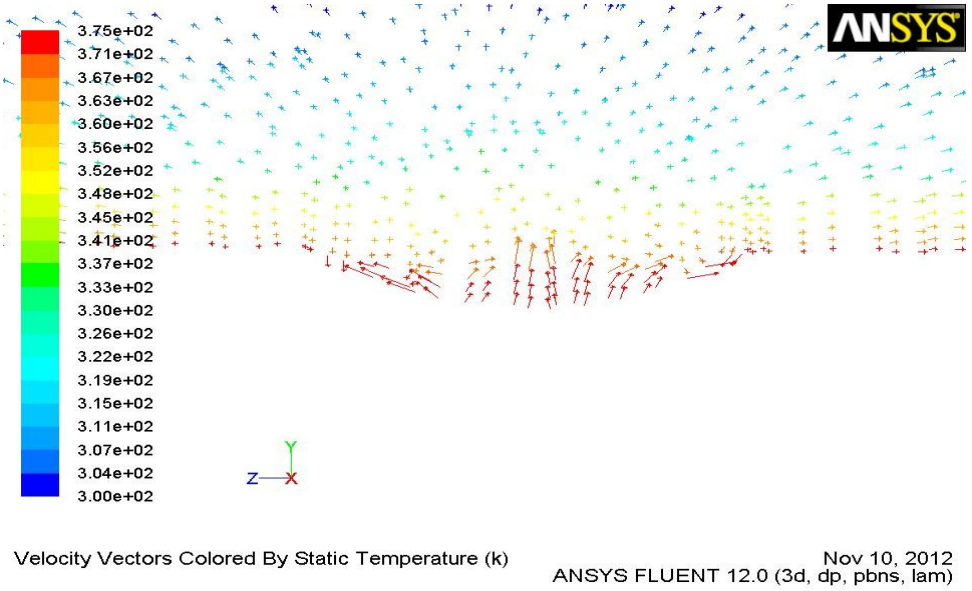

Figure 4-19 Velocity vectors showing secondary flow for inline dimpled array for reynolds number 1000

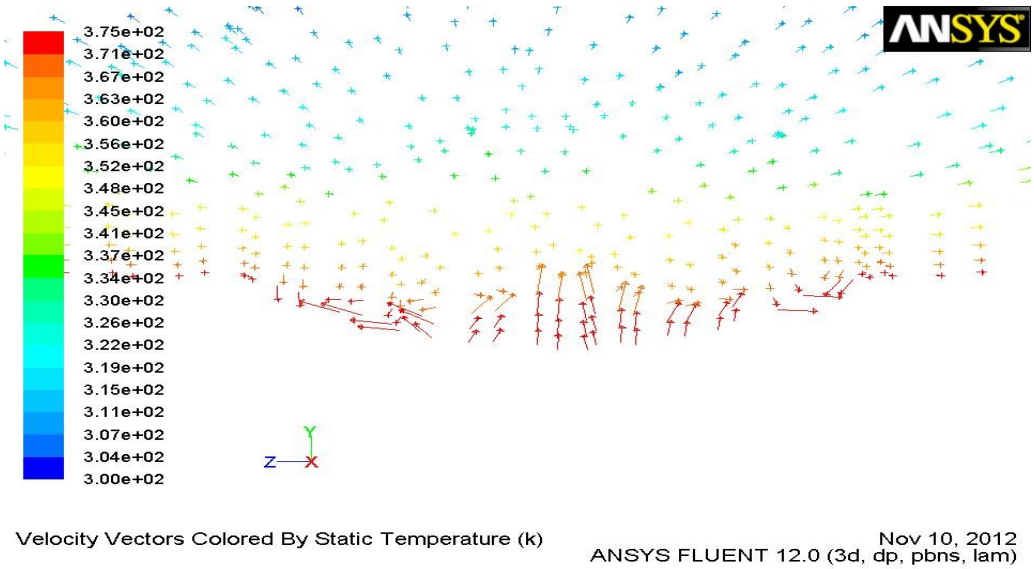

Figure 4-20 Velocity vectors showing secondary flow for inline dimpled array for Reynolds number 1500

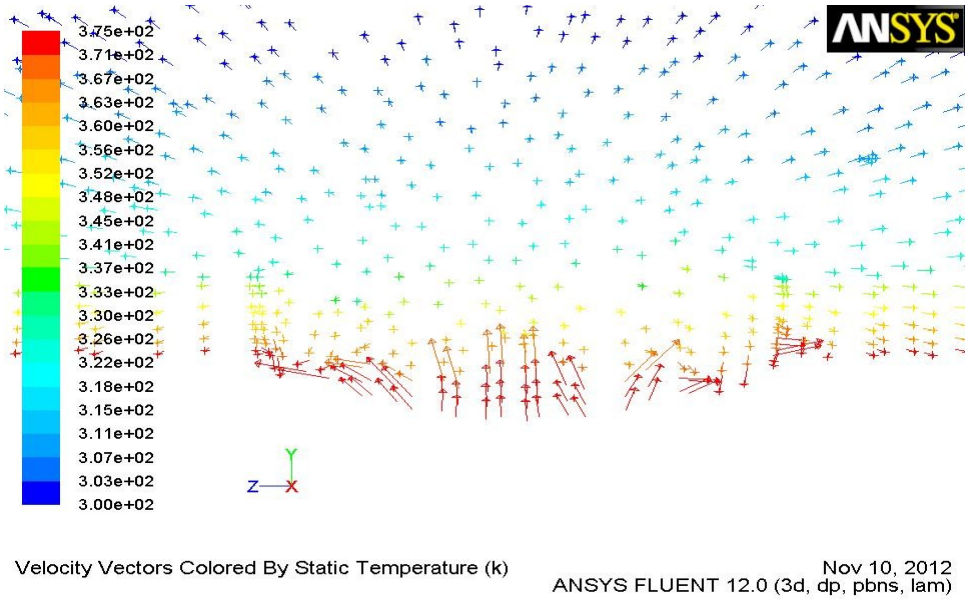

Figure 4-21 Velocity vectors showing secondary flow for staggered dimpled array for Reynolds number 1000

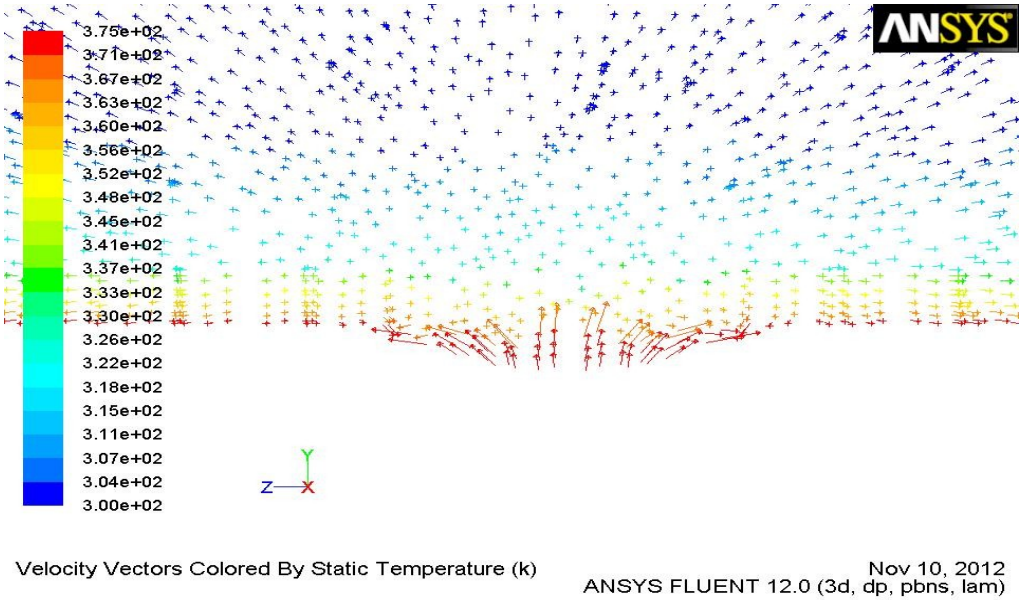

Figure 4-22 Velocity vectors showing secondary flow for staggered dimpled array for Reynolds number 1500

The secondary circulations both at the upstream and downstream end of the dimple are evident from the velocity vectors seen in the span wise direction of the channel. The secondary circulations also increase in strength with increase in Reynolds number.

The reattachment in case of these secondary vortexes is also evident. These secondary vortexes therefore contribute in convective heat transfer enhancement.

Chapter 5

Summary and Conclusions

This study focused on investigating whether the use of dimples can enhance heat transfer characteristics for a closed rectangular channel. Two types of dimpled array geometries on the bottom wall of a channel were tested for 4 different Reynolds numbers ranging from 750 to 1500. The dimple print diameter to depth ratio and the channel height to dimple print diameter ratios were kept constant. The simulation for the study was carried out using the commercial CFD package Fluent.

The comparisons between the two dimple array geometries and the smooth channel was established with parameters like Nusselt number ratio, Heat transfer coefficient ratio, friction factor ratio and Thermal performance factor. The smooth channel data was considered baseline data for evaluating these ratios. The following conclusions were drawn from this study.

1) Heat transfer enhancement in the form of augmented Nusselt number and heat transfer coefficient ratios was observed. $\overline{\mathrm{Nu}} / \overline{\mathrm{Nu}_0}$ values increased with increasing Reynolds number for both dimple array geometries. $\overline{\mathrm{Nu}} / \overline{\mathrm{Nu}_0}$ values varied from about 1.05 to about 1.09 for the staggered array of dimples in the Reynolds number range studied from 750 to 1500. The corresponding $\overline{\mathrm{Nu}} / \overline{\mathrm{Nu}_0}$ values for the inline array of dimples was found in the range of 1.04 to 1.08 suggesting lower levels of heat transfer augmentation for the inline array case. The $\bar{\mathrm{h}}/\overline{\mathrm{h}_0}$ values followed similar trend as the $\overline{\mathrm{Nu}} / \overline{\mathrm{Nu}_0}$ values.
2) The Nusselt number contour plots suggested the need to lower the number of dimples and increase the flat area between them for better

thermal performance. Less or no change in the Nusselt number contour plot on the downstream area on the heated section of the channel for almost all Reynolds number cases indicated that the dimples downstream were majorly contributing to pressure losses and not so much to heat transfer enhancement.

3) The thermal performance factors were plotted for both the dimpled array geometries. The thermal performance values increased with increasing Reynolds number values. Again the thermal performance factor values for the staggered dimpled array geometry were more than corresponding inline dimpled array geometry in the Reynolds number range studied.
4) An insight into the flow structure of the flow over dimpled surfaces in a channel was gained. These low Reynolds number flows over dimpled surfaces led to primary and secondary vortices. The reattachment of the flow on the flat area downstream of the dimple helps in enhancing the convective heat transfer there which is evident from the Nusselt number plots. The secondary vortices also help in enhancing convective heat transfer coefficient as the vortices help in mixing the hot and cold fluids.

Thus, the dimpled surface in the closed channel was found to enhance heat transfer over a smooth channel for laminar airflows. The staggered dimpled array geometry proved to give a better thermal performance than the inline dimpled array.

Chapter 6

Future Recommendations

It can be seen from this study that performance of dimples even in the laminar flow regime depends upon several geometric and other parameters although it can be seen to follow certain consistent trend. There is lots of literature available for thermal performance of dimples in different conditions and for different parameters. Based on this study and available literature, following are a few recommendations for future work.

1) A design optimization study based on dimple geometric parameters such as δ/D, H/D, aspect ratio, dimple array geometry among many others as well as other parameters like Reynolds number should be undertaken to get the most efficient heat sink design for laminar, turbulent as well as transition Reynolds number range.
2) The optimized design needs to be validated using experimental studies.
3) Such kind of dimpled surfaces should be tested in applications like microelectronic cooling where the flow is almost always laminar to give heat transfer enhancement. Even if dimpled heat sinks account for pressure losses, a smaller dimpled heat sink might give same levels of thermal performance as smooth heat sink thus catering to space constraint in such applications.

Appendix A

Nomenclature

H	=	Channel height, (mm)
D	=	Dimple print diameter, (mm)
δ	=	Dimple depth, (mm)
u^*	=	Non dimensional velocity component in x- direction
v^*	=	Non dimensional velocity component in y- direction
w^*	=	Non dimensional velocity component in z- direction
x^*	=	Non dimensional component of length in x- direction
y^*	=	Non dimensional component of length in y- direction
z^*	=	Non dimensional component of length in z- direction
T	=	Temperature
T^*	=	Dimensionless temperature
P	=	Pressure force acting on the face of the fluid element, (N)
L	=	Length of the rectangular channel, (mm)
B	=	Breadth of the channel, (mm)
ρ	=	density of the fluid, (kg/m^3)
μ	=	dynamic viscosity of the fluid, (kg/ m.s)
H_d	=	hydraulic diameter of channel, (m)
k	=	Thermal Conductivity, (W/m·K)
v	=	mean velocity of the fluid, (m/s)
Pe	=	Perimeter of the channel inlet cross section, (m)
A	=	Area of the inlet cross section of channel, (m^2)
Nu	=	Nusselt number
N_{u_0}	=	Nusselt number for a rectangular channel without dimples
$\overline{Nu}$	=	Surface average Nusselt number for the heated surface with dimples
$\overline{N_{u_0}}$	=	Surface average Nusselt number for the smooth heated surface
$\overline{Nu} / \overline{Nu_0}$	=	Average Nusselt number ratio,

p	=	static pressure, (Pa)
Pr	=	Prandtl number
T_{in}	=	Temperature at the inlet, (K)
T_{wall}	=	Temperature at the heated wall, (K)
Re	=	Reynolds number, (dimensionless)
T_{wall}	=	Temperature at the heated wall, (K)
h	=	convective heat transfer coefficient, (W/m^2K)
Q	=	Heat flux, (W)
A_t	=	Heat transfer surface area
ΔT	=	Temperature difference between solid surface and fluid area, (K)
$\bar{h}$	=	Surface average heat transfer coefficient of the heated surface with dimples, (W/m^2K)
$\overline{h_0}$	=	Surface average heat transfer coefficient of the heated surface without dimples, (W/m^2K))
h_f	=	head loss in the channel, (m)
f_D	=	Darcy friction factor
g	=	local acceleration due to gravity, (m^2/s)
Δp	=	Pressure loss in the channel, (Pa)
TP	=	Thermal performance factor

References

[1] Anonymous "Http://www.Faqs.org/sports-science/Fo-Ha/Golf-Ball-Construction-and-Flight-Dynamics.html#b," .

[2] Afanasyev, V., Chudnovsky, Y. P., Leontiev, A., 1993, "Turbulent Flow Friction and Heat Transfer Characteristics for Spherical Cavities on a Flat Plate," Experimental Thermal and Fluid Science, 7(1) pp. 1-8.

[3] Anderson, J.D., 1995, "Computational fluid dynamics," McGraw-Hill, .

[4] Bearman, P., and Harvey, J., 2012, "Control of Circular Cylinder Flow by the use of Dimples," AIAA Journal, 31(10) .

[5] Bunker, R. S., and Donnellan, K. F., 2003, "Heat Transfer and Friction Factors for Flows Inside Circular Tubes with Concavity Surfaces," Transactions of the ASME-T-Journal of Turbomachinery, 125(4) pp. 665-672.

[6] Burgess, N., and Ligrani, P., 2004, "Effects of dimple depth on Nusselt numbers and friction factors for internal cooling in a channel," Anonymous ASME, .

[7] Chyu, M., Yu, Y., Ding, H., 1997, "Concavity Enhanced Heat Transfer in an Internal Cooling Passage," 7, pp. 1997.

[8] Doo, J., Yoon, H., and Ha, M., 2010, "Study on Improvement of Compactness of a Plate Heat Exchanger using a Newly Designed Primary Surface," International Journal of Heat and Mass Transfer, 53(25) pp. 5733-5746.

[9] Franke, K., 2008, "Http://www.Oobgolf.com/content/columns/know+the+game/1-1675-Why_Does_A_Golf_Ball_Have_Dimples.Html,".

[10] Han, J. C., 2006, "Turbine Blade Cooling Studies at Texas A&M University: 1980-2004," Journal of Thermophysics and Heat Transfer, 20(2) pp. 161-187.

[11] Isaev, S., Leont'ev, A., and Baranov, P., 2000, "Identification of Self-Organized Vortexlike Structures in Numerically Simulated Turbulent Flow of a Viscous

Incompressible Liquid Streaming Around a Well on a Plane," Technical Physics Letters, 26(1) pp. 15-18.

[12] Isaev, S., and Leont'ev, A., 2003, "Numerical Simulation of Vortex Enhancement of Heat Transfer Under Conditions of Turbulent Flow Past a Spherical Dimple on the Wall of a Narrow Channel," High Temperature, 41(5) pp. 665-679.

[13] Isaev, S., and Leont'ev, A., 2003, "Numerical Simulation of Vortex Enhancement of Heat Transfer Under Conditions of Turbulent Flow Past a Spherical Dimple on the Wall of a Narrow Channel," High Temperature, 41(5) pp. 665-679.

[14] Isaev, S., Leont'ev, A., Baranov, P., 2001, "Numerical Analysis of the Effect of Viscosity on the Vortex Dynamics in Laminar Separated Flow Past a Dimple on a Plane with Allowance for its Asymmetry," Journal of Engineering Physics and Thermophysics, 74(2) pp. 339-346.

[15] Isaev, S., Leont'ev, A., Metov, K. T., 2002, "Modeling of the Influence of Viscosity on the Tornado Heat Exchange in Turbulent Flow Around a Small Hole on the Plane," Journal of Engineering Physics and Thermophysics, 75(4) pp. 890-898.

[16] Isaev, S., Pyshnyi, I., Usachov, A., 2002, "Verification of the Multiblock Computational Technology in Calculating Laminar and Turbulent Flow Around a Spherical Hole on a Channel Wall," Journal of Engineering Physics and Thermophysics, 75(5) pp. 1155-1158.

[17] Kim, K. Y., and Choi, J. Y., 2005, "Shape Optimization of a Dimpled Channel to Enhance Turbulent Heat Transfer," Numerical Heat Transfer, Part A: Applications, 48(9) pp. 901-915.

[18] Ligrani, P., Mahmood, G., Harrison, J., 2001, "Flow Structure and Local Nusselt Number Variations in a Channel with Dimples and Protrusions on Opposite Walls," International Journal of Heat and Mass Transfer, 44(23) pp. 4413-4425.

[19] Lin, Y., Shih, T., and Chyu, M., 1999, "Computations of Flow and Heat Transfer in a Channel with Rows of Hemispherical Cavities," ASME Paper, (99-GT) pp. 263.

[20] M.Y. Blen'kiy, M.A. Gotovskiy, B.M. Lekakh, B.S. Fokin, K.S. Dolgushin, 1994, pp. 196.

[21] Mahmood, G., Hill, M., Nelson, D., 2001, "Local Heat Transfer and Flow Structure on and Above a Dimpled Surface in a Channel," Journal of Turbomachinery, 123(1) pp. 115-123.

[22] Mahmood, G., and Ligrani, P., 2002, "Heat Transfer in a Dimpled Channel: Combined Influences of Aspect Ratio, Temperature Ratio, Reynolds Number, and Flow Structure," International Journal of Heat and Mass Transfer, 45(10) pp. 2011-2020.

[23] Mahureand, A., and Kriplani, V., 2012, "Review of Heat Transfer Enhancement Techniques," International Journal of Engineering, 5(3) pp. 241-249.

[24] Moon, H., O'Connell, T., and Glezer, B., 2000, "Channel Height Effect on Heat Transfer and Friction in a Dimpled Passage," Journal of Engineering for Gas Turbines and Power, 122pp. 307.

[25] Park, J., Desam, P., and Ligrani, P., 2004, "Numerical Predictions of Flow Structure Above a Dimpled Surface in a Channel," Numerical Heat Transfer, Part A: Applications, 45(1) pp. 1-20.

[26] Patankar, S. V., and Spalding, D. B., 1972, "A Calculation Procedure for Heat, Mass and Momentum Transfer in Three-Dimensional Parabolic Flows," International Journal of Heat and Mass Transfer, 15(10) pp. 1787-1806.

[27] Rao, Y., Wan, C., and Xu, Y., 2012, "An Experimental Study of Pressure Loss and Heat Transfer in the Pin Fin-Dimple Channels with various Dimple Depths," International Journal of Heat and Mass Transfer, .

[28] Silva, C., Marotta, E., and Fletcher, L., 2007, "Flow Structure and Enhanced Heat Transfer in Channel Flow with Dimpled Surfaces: Application to Heat Sinks in Microelectronic Cooling," Journal of Electronic Packaging, 129(2) pp. 157-166.

[29] Small, E., Sadeghipour, S. M., and Asheghi, M., 2006, "Heat Sinks with Enhanced Heat Transfer Capability for Electronic Cooling Applications," Journal of Electronic Packaging, 128(3) pp. 285-290.

[30] Terekhov, V., Kalinina, S., and Mshvidobadze, Y. M., 1997, "Heat Transfer Coefficient and Aerodynamic Resistance on a Surface with a Single Dimple," Journal of Enhanced Heat Transfer, 4(2) .

[31] Terekhov, V., Kalinina, S., and Mshvidobadze, Y. M., 1995, "Flow Structure and Heat Transfer on a Surface with a Unit Hole Depression," Russ.J.Eng.Thermophys, 5(11) .

[32] Turnow, J., Kornev, N., Zhdanov, V., 2012, "Flow Structures and Heat Transfer on Dimples in a Staggered Arrangement," International Journal of Heat and Fluid Flow, .

[33] Xiao, N., Zhang, Q., Ligrani, P. M., 2009, "Thermal Performance of Dimpled Surfaces in Laminar Flows," International Journal of Heat and Mass Transfer, 52(7) .

[34] Y.F Gortyshov, I.A. Popov, R.D. Amirkhanov, K.E. Gulitsky, 1998, "11th International Heat Transfer congress," Anonymous 6, pp. 83.

Biographical Information

Abhijit Paranjape was born in Mumbai, India. He earned his Bachelor's degree in Mechanical engineering from the University of Mumbai in June 2010. His interests in Mechanical engineering include CFD, FEA, Fluid Mechanics, Heat Transfer and Optimization. Upon completion of is masters, he would like to pursue his career as a Mechanical engineer in industry.